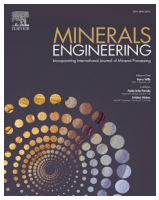
Minerals Engineering 228 (2025) 109308



Contents lists available at ScienceDirect

Minerals Engineering

journal homepage: www.elsevier.com/locate/mineng





Upscaling and optimization of reagents systems in froth flotation: A DoE and numerical-optimization-based methodology

B. Ben Said [a,b,*], M. Rudolph [a], D. Goldmann [b], L. Pereira [a]

[a] Helmholtz-Zentrum Dresden-Rossendorf, Helmholtz-Institute Freiberg for Resource Technology, Chemnitzer Straße. 40, 09599 Freiberg, Germany
[b] Institute of Mineral and Waste Processing, Recycling and Circular Economy Systems, Walther-Nernst-Straße 9, D-38678 Clausthal-Zellerfeld, Germany

ARTICLE INFO

Keywords:
Flotation process
Reagent systems
Upscaling
Process optimization
Design of experiments
Grade-recovery-performance index
Mini pilot plant

ABSTRACT

We introduce a unique approach for faster and more systematic optimization and upscaling of reagent systems in froth flotation processes. By integrating the statistical design of experiments with numerical optimization techniques, our method ensures a seamless transition from laboratory experimentation to pilot and industrial-scale implementation. This approach uses comprehensive lab-scale experimental data to assign the effects of reagent system operating parameters and pre-identify optimal conditions. These predictions streamline the optimization algorithm for continuous process improvement, minimizing its convergence issues and, consequently, the test work time and resource consumption.

We validated this methodology with a case study on a low-grade scheelite ore, demonstrating a reduction of 60 % in required test work at pilot scale. A four-day industrial campaign resulted in a 16 % increase in concentrate grade without hindering recovery. Additionally, we discuss the influence of variations in ore feed properties on froth flotation performance while optimizing the reagent system. Within this context, we introduce the Grade-Recovery-Performance (GRP) index, a two-dimensional metric to quantify the performance of separation processes according to grade and recovery simultaneously.

1. Introduction

The mining industry aims to enhance its economic viability and ecological sustainability, while at the same time facing a growing complexity of orebodies. The primary objective is to boost mineral concentrate grade and recovery while simultaneously reducing energy and resource consumption (Evans et al., 2009; Jang and Topal, 2020).

Froth flotation is the predominant process in the mining industry, with flotation reagents playing a crucial role in determining its performance (Yan et al., 2013; Gao et al., 2020). Yet, given the time and costs associated with metallurgical test work, the understanding of reagents influence on froth flotation performance primarily stems from small-scale studies. Results from microflotation tests do not seamlessly translate to batch flotation operations due to simplifications regarding the flotation process (e.g., modifications to cell hydrodynamic conditions) and the complexities of real ores (e.g., use of pure minerals instead of complex particles). Furthermore, despite numerous studies on reagent system optimization at the batch laboratory scale (Sheridan et al., 2002; Kalyani and Pallavika, 2005; Martínez-L et al., 2003), their industrial application remains a challenge. Transitioning from batch to continuous operation necessitates considerations of factors such as reagent dosage, which is typically reduced due to stream recirculation, and integration with other process units, which can significantly affect the overall performance (Loveday and Brouckaert, 1995; Maldonado et al., 2007). Moreover, froth flotation is characterized by an intricate interplay between chemical and hydrodynamic parameters, which further complicates optimization efforts by leading to an enormous number of process conditions to be tested (Sajjad and Otsuki, 2022; Szmigiel et al., 2024). Consequently, the selection of reagents and optimization of dosages in flotation are largely informal, subjective, and empirical, where only a couple of variables is tested based on experience (Nagaraj, 2005).

Given this practice, Nagaraj (Nagaraj, 2005) proposed a holistic approach for reagent selection and optimization in flotation processes. It begins with a discovery-definition step where clear objectives are set, plant operations are assessed, and key factors (e.g., constraints, ore types, and success criteria) are considered. The second step involves reagent selection based on technical factors like reagent chemistry, ore types, and compatibility with other reagents. The third phase introduces

* Corresponding author at: Department of Processing, Helmholtz-Institute Freiberg for Resource Technology, Helmholtz-Zentrum Dresden-Rossendorf, Chemnitzer Straße 40, Freiberg, Germany.
E-mail address: b.ben-said@hzdr.de (B. Ben Said).

https://doi.org/10.1016/j.mineng.2025.109308
Received 11 September 2024; Received in revised form 6 April 2025; Accepted 8 April 2025
Available online 16 April 2025
0892-6875/© 2025 The Author(s). Published by Elsevier Ltd. This is an open access article under the CC BY license (http://creativecommons.org/licenses/by/4.0/).

laboratory and plant testing, using statistical experimental design in laboratory scale to identify conditions for plant testing and potential threats or benefits.

While the author claims that true optimization occurs in the plant, this approach falls short in bridging the gap between batch and continuous operation and conditions in terms of dimensions and recirculation. It also lacks a systematic method for applying lab-scale scenarios to the plant. The proposed approach is more of a conceptual framework rather than a set of detailed techniques for ensuring smooth optimization and scaling of reagents in froth flotation, particularly for a successful transition from batch to continuous operation. Furthermore, the approach can be daunting and time-consuming at both lab and industrial scales, considering the required energy and resources, and it does not reduce the possibility of harmful industrial trials. In addition to the optimization strategy used, the definition of a cost function is fundamental to the quality of an optimization routine. Separation processes are typically evaluated by two or more parameters, simultaneously (Drzymala et al., 2010). The Fuerstenau upgrading plot, for example, relates the recovery of the ore component in the concentrate to the recovery of the remaining gangue components in the tailings. It has been successfully used in different laboratory and industrial studies (Drzymala et al., 2010). Halbich (grade-recovery) curves are also typically used to evaluate the outcome of mineral beneficiation activities. It offers a distinct advantage over other upgrading curves by effectively linking two crucial separation parameters: recovery and grade (Drzymala et al., 2013). An improvement in flotation performance is typically reflected by an upwards and/or rightward shift in the grade-recovery curve, indicating higher recovery at a given grade or higher grade at a given recovery (Drzymala et al., 2013; Neethling and Cilliers, 2012; Napier-Munn, 2012). Such shifts are desirable outcomes in mineral beneficiation processes, as they represent enhanced separation efficiency. However, this evaluation is typically qualitative, and therefore not suited for process optimization. Napier-Munn et al. (Napier-Munn, 1998) proposed comparing recovery-grade regression lines in plant trials by fitting linear regressions to recovery-grade data and analyzing their gradients and mean separation. He emphasized the need for numerous observations due to the absence of formal experimental design and reliance on natural grade fluctuations. Additionally, he cautioned that differences in residual mean squares could compromise the reliability of comparisons.

In this contribution, we propose a unique approach to process optimization and upscaling. It combines statistical experimental design — to refine the parameter space and to understand the interdependence of process parameters — and numerical optimization using the Nelder-Mead optimization method— to optimize the process at full scale. This combination enables a faster and systematic upscaling and optimization of reagent systems in flotation processes, minimizing the risk of non-convergence of the optimization algorithm without adding too much to the test work required. The approach is demonstrated in the upscaling of colloidal silica as a depressant for calcite in scheelite flotation (Kupka and Babel, 2020). Additionally, we propose the Grade-Recovery-Performance (GRP) flotation index, which jointly quantifies improvements in grade and recovery for mineral concentration activities.

2. Material and methods

2.1. Methodological framework

This study outlines a comprehensive methodology for refining and optimizing flotation processes, extending beyond the specific case of the scheelite ore case. Initially, micro and batch flotation experiments were conducted using a Design of Experiments (DoE) approach to systematically refine the parameter space. Based on these batch-scale results, the Nealder Mead optimization method was then applied to continuous pilot experiments, simplifying the algorithm, identifying an optimal range, and assessing potential risks before progressing to industrial trials. Finally, this optimized approach was tested in industrial trials, with the flotation of scheelite ore using novel depressants serving as the case study.

2.2. Reagents

The collector used for batch flotation experiments was sodium oleate $C_{18}H_{33}NaO_2$ (NaOl) from Carl Roth with a purity of 90 %. pH modifiers are hydrochloric acid (HCl) and sodium hydroxide (NaOH) from Carl Roth GmbH, and frother is 4-methyl-2-pentanol (MIBC) supplied by Alfa Aesar. Seven types of Levasil® Colloidal Silica (CS) provided by Nouryon® were tested as calcite depressants, differing in modification and specific surface area/particle size, as summarized in Table 1.

2.3. Design of experiments

Design of experiments (DoE) is a statistical technique to gain insight into a process by quantifying the effect of process variables on the measured process response and to get statistically validated relationships between these process variables with a minimal number of experiments. DoE is widely used for optimization tasks (Durakovic, 2017). Using different types of DoEs, batch flotation tests were conducted according to a workflow composed of three stages: (1) screening; (2) investigation and modelling; and (3) verification and optimization (Ben Said et al., 2022).

As the name implies, the purpose of the screening phase is to screen out process parameters that have no significant effect on the response variable. Fractional factorial design is the most common design type utilized for screening (Durakovic, 2017). This design is employed, especially when numerous process parameters need to be investigated, but using a full factorial design would be too expensive and time-consuming. A portion of the total runs from a full factorial design are carried out. Since only a part of the experimental volume is covered in the screening phase, some effects are confounded (i.e. the impacts of two or more variables cannot be disentangled), resulting in a loss of resolution. Resolution describes how far the effects in a fractional factorial design are aliased (Durakovic, 2017).

In the investigation and modelling phase, a full-factorial DoE is carried out using the significant process parameters after the irrelevant ones have been screened out. Testing every possible combination of the independent process parameters and how it affects the response variables is the aim. Both main and two-factor interaction effects are evaluated, and the data set is fitted with a model assumption based on the residual's analysis. To determine whether the assumed model has a curvature, a centre point is added to the design.

Central composite designs are extensions of the factorial experimental designs. They are composed of a partial factorial or full factorial experimental design and a so-called CCD star with a central experiment whose extreme settings go beyond those of the factorial experimental design. A central composite experimental design is suitable for studying quadratic relations (Ahn, 2015). To ensure a minimum number of experiments and maximum flexibility, the central composite design composes the workflow as part of the verification of the assumed model. It is

Table 1
Summary of colloidal silica suspensions and their specifications. *Calculated from the specific surface area.

Specific surface area($\frac{m^2}{g}$)	Modification (—)	Particle size* (nm)	Acronym
250	None	9	N_250
500	None	4.5	N_500
220	Silane	10	S_220
500	Silane	4.5	S_500
250	Aluminate	9	Al_250
500	Aluminate	4.5	Al_500
1100	Aluminate	2	Al_1100

assumed that the full factorial experimental design with centre points already performed is sufficiently ample to estimate curvature effects. Once the model is established and verified, the process can be numerically optimized.

2.4. Nelder Mead simplex method

The Nelder-Mead simplex algorithm, also known as the downhill simplex method, is an optimization technique which is often employed for non-linear optimization problems where the goal is to minimize (or maximize) a real-valued function (Nelder and Mead, 1965; Baudin, 2009). The Method is especially effective when the function to be optimized is not consistently smooth or differentiable. The algorithm starts with an initial simplex, a geometric shape in the parameter space, consisting of n + 1 vertices, where n is the number of parameters to be optimized. Each vertex represents a candidate solution, and the function is evaluated at each point. The vertices are then ranked based on the function values, with x_{n+1} being the worst vertex. The algorithm iteratively improves the simplex by applying transformation steps as described below.

i. Centroid calculation (x_c)

The centroid is calculated as the average of all the n vertices, excluding the worst vertex:

$$x_c = \frac{1}{n}\sum_{i=1}^{n} x_i \tag{1}$$

where x_i are the best n vertices of the simplex.

ii. Reflexion (x_r)

The worst vertex x_{n+1} is reflected through the centroid x_c to generate a new point:

$$x_r = x_c + \alpha(x_c - x_{n+1}) \tag{2}$$

where α is the reflection coefficient set typically between 0.5 and 1.

- If $f(x_r)$ is better than the second-worst vertex but not the best, x_{n+1} is replaced with x_r.
- If $f(x_r)$ is better than the current best point, the algorithm attempts expansion.

iii. Expansion (x_e)

If the reflected vertex x_r is better than best vertex, the simplex is expanded in the direction of the reflection:

$$x_e = x_c + \gamma(x_r - x_c) \tag{3}$$

where γ is the expansion coefficient set typically between 1.5 and 2.

- If $f(x_e)$ is better than $f(x_r)$, x_{n+1} is replaced by x_e.
- Otherwise, x_r is used instead.

iv. Contraction (x_{oc} and x_{ic})

If $f(x_r)$ is worse than the second-worst vertex, the algorithm contracts the simplex.

a) Outside contraction (x_{oc})

If $f(x_r)$ is worse than the second-worst point but still better than the worst vertex, the worst vertex is moved towards the reflected point:

$$x_{oc} = x_c + \beta(x_r - x_c) \tag{4}$$

where β is the contraction coefficient set typically between 0.5 and 1.

b) Inside contraction:

If $f(x_r)$ is worse than even the worst vertex x_{n+1}, the simplex is contracted inward towards the centroid:

$$x_{oc} = x_c - \beta(x_c - x_{n+1}) \tag{5}$$

- If contraction improves the function value, x_{n+1} is replaced.
- If contraction fails to improve the function value, shrinkage is applied.

v. Shrinkage

If neither reflection nor contraction leads to improvement, the simplex is shrunk toward the best point x_1:

$$x'_i = x_1 + \delta(x_i - x_1), \forall i = 2, \cdots, n+1 \tag{6}$$

where δ is the shrinkage coefficient set typically between 0.5 and 1.

A visual representation of these operations is illustrated in Fig. 1.

The algorithm repeats these steps until it meets a termination criterion, such as a maximum number of iterations or a pre-defined convergence tolerance. The NM algorithm is implemented within the pilot and industrial tests in the framework of the proposed approach.

2.5. Flotation experiments

2.5.1. Microflotation of scheelite and calcite

Single mineral flotation experiments were carried out on pure scheelite and calcite with the three colloidal silica dispersions types namely the non-functionalized, the aluminate modified and the silane modified colloidal silica at a sodium oleate concentration of 10^{-3} mol/l, pH 8 and a specific surface area of colloidal silica of 500 m^2/g. A mixture of 160 ml aqueous solution with 10 mM KCl and one gram of each mineral was agitated at 400 rpm in a beaker. First, a two-minute pH conditioning period was conducted using 1 M HCl or NaOH feedstock solutions, respectively. Depressant and collector conditioning followed sequentially, each lasting three minutes at 400 rpm. The suspension was then transferred to the Hallimond tube and agitated at 800 rpm for two minutes. Microflotation was conducted for two minutes at a 20 cm^3/min airflow rate. The collected concentrates and tailings were filtered and dried overnight at 50 – 60 °C.

2.5.2. Batch and pilot scale experiments

2.5.2.1. Ore mineralogy. A low-grade scheelite ore under investigation

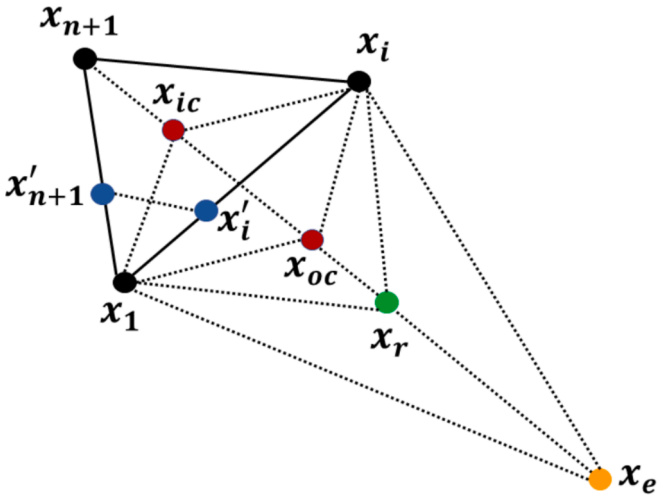


Fig. 1. Visual representation of the Nelder-Mead algorithm's operations on a simplex in two dimensions.

contains 1.1 % (w/w) calcite and 0.5 % (w/w) scheelite, as shown in Fig. 2. Quartz, plagioclase, and hornblende are the primary gangue minerals, which together make up 77.5 % (w/w) of the ore. Ore samples were collected in the processing plant directly after the final milling stage, being its particle size distribution suitable for flotation ($d_{80,3}$ = 170 μm). For each test, 500 g samples were split using a Retsch PT100. Before each flotation test, the ore was mixed with 300 mL of water and ground in a lab rod mill having a critical rotational speed of 121 rpm to freshen up particle surfaces. The ore was ground for 3 min at 96 rpm which correspond to a relative critical rotation of 79 %. The rod mill has a critical speed of 121 rpm. Froth flotation tests were conducted in a 1.5 L Magotteaux® bottom-driven flotation cell, with an active pulp volume (excluding the rotor–stator assembly) of 1.2 L. The tests were performed at a pulp density of 33 %, an impeller speed of 450 rpm, and an airflow rate of 5 L/min.

2.5.2.2. Batch flotation procedure and experimental conditions. The conditioning scheme is illustrated in Fig. 3.Within time intervals of [0;60] s, [60;180] s, and [180;420] s, three concentrates were collected, i.e. a kinetic flotation test is conducted. The froth was scraped every five seconds. The filtered flotation products were dried overnight at 50-60 °C in a drying oven, and mass recoveries were calculated based on dry weights. All samples were split and then analyzed with a Bruker S1 TITAN 800 portable XRF (pXRF). To translate pXRF results into mineralogical compositions based on an element-to-mineral conversion methodology (Ben Said et al., 2024), a few samples were examined using XRD and the Mineral Liberation Analyzer (MLA) (Fandrich et al., 2007).

First, a fractional factor experimental design was used. The process variables pH, collector dosage, frother dosage and colloidal silica dosage were analysed. To simplify the experimental design and minimize the number of runs, the specific surface area was first set at 500 m^2/g. Table 2 shows the varied parameters of the screening phase. The experimental plan was carried out for the three CS modifications.

Two experimental phases were carried out following the screening stage, where it was determined that the frother dosage had no significant effect on the relevant target variables and, consequently, fixed at a dosage of 0.17 mmol/L during the investigation phase. Full factorial design of experiments was used to conduct the experiments. The variables in the first stage (Table 3), which represent the reference blank test, were the pH and the dosage of sodium oleate. The effect of the colloidal silica dosage, pH, sodium oleate dosage, and colloidal silica dosage were the process parameters investigated in the second stage

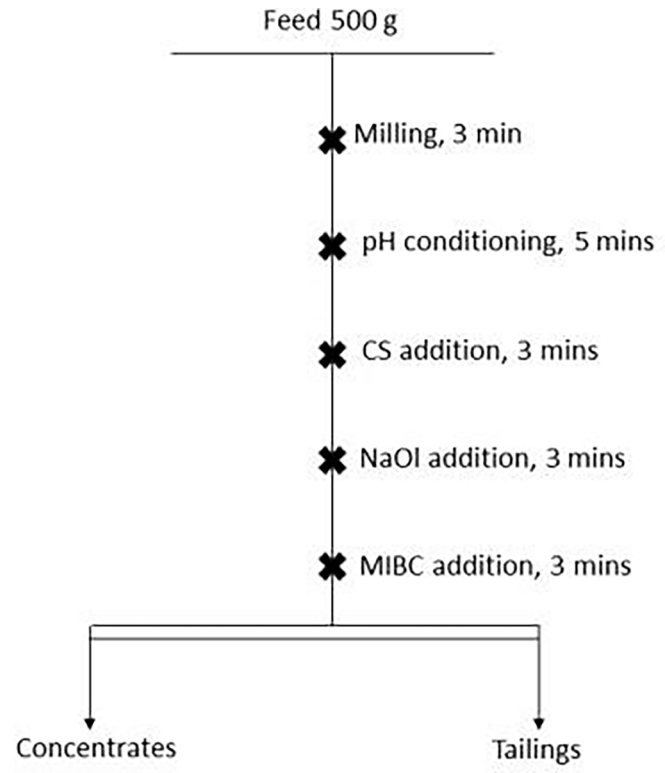


Fig. 3. Froth flotation flow chart of low-grade scheelite ore.

Table 2
Levels of variables investigated for the screening phase (4 fractional factorial design). These process conditions were applied separately to each of the colloidal silica modifications.

Parameter	Unit	Factor level	
		minimum	maximum
pH	–	8	10
Collector dosage	g/t	100	400
Depressant dosage	g/t	100	500
Frother dosage	mmol/L	0.10	0.24

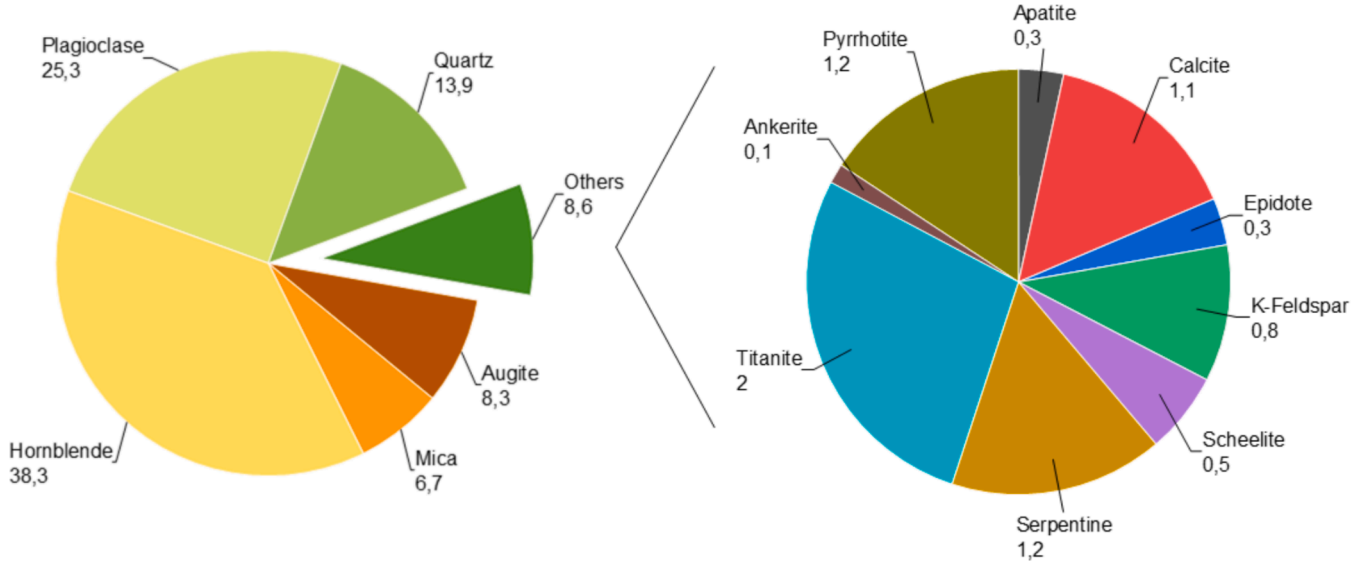


Fig. 2. Mineralogical composition of the ore in % (w/w) obtained by quantitative X-ray diffraction (XRD) and mineral liberation analyser (MLA).

Table 3
Levels of variables investigated for the blank tests (2^2 full factorial design).

Parameter	Unit	Factor level	
		minimum	maximum
pH	–	8	10
Collector dosage	g/t	100	400

Table 4
Levels of variables investigated for the tests with colloidal silica (2^3 full factorial design). These process conditions were applied separately to each of the colloidal silica modifications.

Parameter	Unit	Factor level	
		minimum	maximum
pH	–	8	10
Collector dosage	g/t	100	400
Depressant dosage	g/t	50	550

(Table 4), which was carried out for each colloidal silica suspension.

The main and interaction effects of the process parameters, as well as their statistical significance, were calculated by creating and evaluating an experimental plan with the open-access R-Shiny platform developed in-house (Ben Said et al., 2022).

2.5.2.3. Pilot scale flotation. Pilot-scale flotation tests were conducted using a CPT Mini Pilot Plant from Eriez®, featuring a cell volume of 1.7 L per flotation stage. The flotation circuit, illustrated in Fig. 4, consisted of four rougher stages and three cleaner stages, is. The first cell of the machine was designed for conditioning. Tailings from the first and second cleaner stages were recirculated to the rougher stage, while tailings from the third cleaner stage were recirculated to the first cleaner stage. No scavenger stage was employed, meaning the tailings from the rougher stages constituted the final tailings. The feed, with a 33 % solid content, was processed at 10 kg/h. The slurry had a specific gravity of 1.28 g/cm^3, with the feed ore having specific gravity of 2.9 g/cm^3. The slurry was fed at a flow rate of 400 mL/min, corresponding to a liquid flow of approximately 341 mL/min. pH was measured and controlled in both the first rougher stage and the first cleaner stage. Each test required approximately 2.5 to -3 h to reach a steady state, which was defined as the point where the time-dependent increase in the masses of the final concentrate and tailings became nearly constant. Once steady state was achieved, one-minute samples were taken from each stream. The samples were filtered and dried overnight at temperatures between 50 °C and 60 °C. All samples were split and analysed using a Bruker S1 TITAN 800 portable XRF (pXRF). Mass balances were performed in Excel.

2.5.2.4. Approach and link between batch and continuous scale flotation. Optimizing continuous batch operations using numerical optimization methods, such as the NM algorithm, can be time and energy-consuming due to the high number of parameters involved. To address the challenge of managing numerous vertices in the starting simplex, the NM algorithm is simplified based on insights from batch flotation results. Parameters that have been shown to be have minimal impact on process performance or are not of primary interest are treated as pre-optimized and are varied only within a narrow range around their established optimal values. Meanwhile, parameters that significantly affect the process or are of particular interest, such as colloidal silica dosages in this case, are varied freely within defined constraints (e.g., no negative dosage values).

This simplification reduces the starting simplex of the NM algorithm to m + 1 component, where m represents the number of parameters considered of interest, out of the full parameter space consisting of n variables. The effectiveness of this approach is investigated in this study by comparing the simplified scheme (m + 1 vertices) with the full scheme (n + 1 vertices).

2.5.3. Industrial-scale flotation

A four-day industry campaign was conducted using the NM optimization algorithm, utilizing the optimal parameter settings identified at the pilot scale. The initial vertices of the simplex were selected and set within the pre-identified optimal ranges at the pilot scale. To evaluate the outcomes, the GRP index was implemented, allowing the assessment of process results in two dimensions: scheelite grade and recovery. Each test lasted 2 h. Additionally, a separate test was performed using the

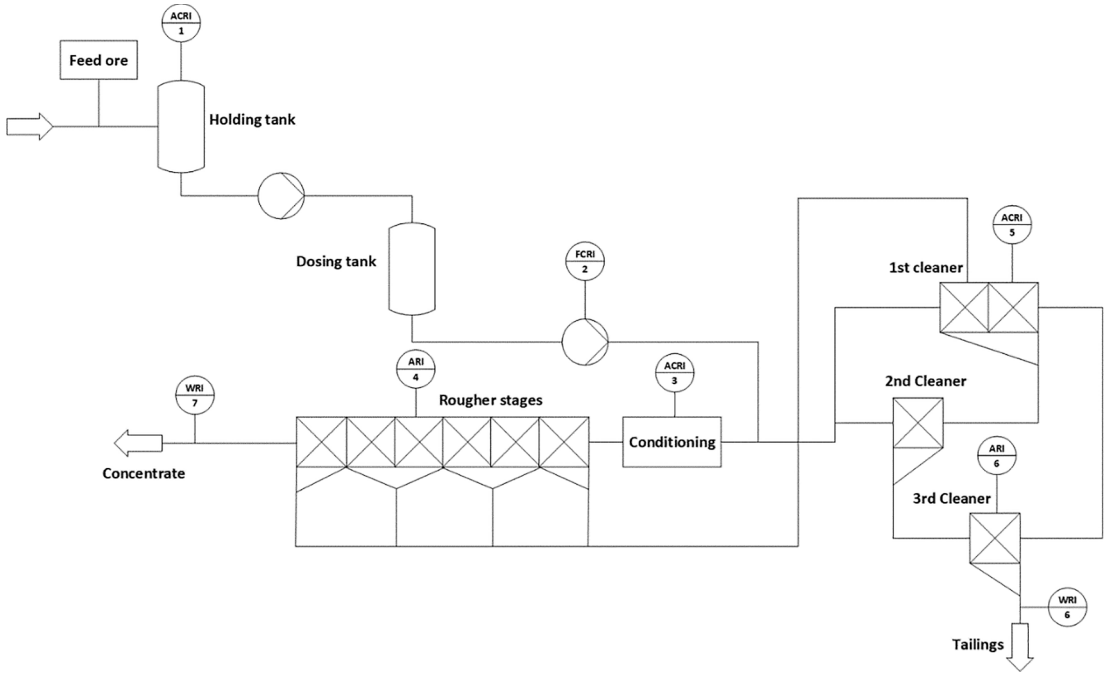


Fig. 4. Flotation circuit of the pilot scale consists of four rougher stages and three cleaner stages. pH was measured and controlled in both the first rougher stage and the first cleaner stage, and only measured in the third rougher and cleaner stages. The masses of the final concentrate and tailings were measured.

optimal parameter settings for a duration of 4 h after extraction activities, to assess the impact of feed ore properties on the process performance. After each trial, samples were collected at every stage. All samples were analysed using a Bruker S1 TITAN 800 portable XRF (pXRF). Furthermore, samples from the benchmark process and the trials with optimal parameter settings before and after the extraction activities were analysed with XRD and MLA.

2.6. Grade-Recovery performance index

The Grade-Recovery-Performance-Index serves to assess the efficacy of concentration processes in multiple dimensions simultaneously. Given the different characteristics of batch and continuous operations, a unique GRP index was developed for each mode of operation.

2.6.1. Batch operation

The GRP index is composed of two primary indices. The first is the Absolute Grade-Recovery index (AGR), which serves as an indicator of the distance between the curve and the zero point. This value provides insights into the total performance in terms of both dimensions (grade and recovery), without bias towards any of the process metrics. Mathematically, this distance is the sum of the distances from the maximum grade and recovery to the zero point. Visually, these distances represent the hypotenuses of the red and green triangles, as illustrated in Fig. 5 and formulated in Equation (7):

$$AGR = \left(G_{min,n}{}^2 + R_{max,n}{}^2\right)^{1/2} + \left(G_{max,n}{}^2 + R_{min,n}{}^2\right)^{1/2} \quad (7)$$

where $G_{min,n}$, $G_{max,n}$, $R_{min,n}$, and $R_{max,n}$ are respectively the minimum and maximum grades and recoveries observed in the kinetic batch experiment under condition n.

For comparability of the two dimensions, the values for grade and recovery are normalised with the maximum grades and recoveries observed in the entire testing campaign.

The second index is the Equilibrium Grade-Recovery index (ERG), which indicates the position of the curve in relation to the cumulative grade axis and the cumulative recovery axis, respectively. This gives insights into which process parameter dominates the results. It is the quotient of the two hypotenuses of the triangles illustrated in Fig. 5, mathematically represented in Equation (8).

$$EGR = \left(G_{min,n}{}^2 + R_{max,n}{}^2\right)^{1/2} / \left(G_{max,n}{}^2 + R_{min,n}{}^2\right)^{1/2} \quad (8)$$

Two possible scenarios can arise:

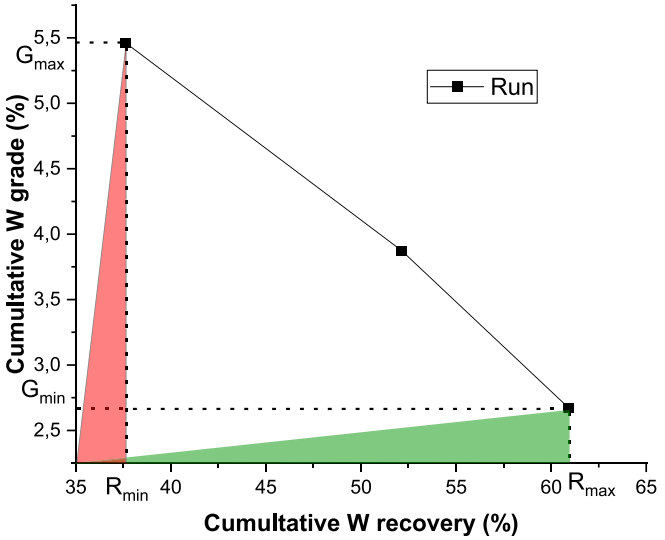


Fig. 5. Graphical visualization for the calculation of the GRP index.

i. EGR > 1 implies that the recovery dimension is dominant over the grade dimension.
ii. EGR < 1 implies that the grade dimension is dominant over the recovery dimension.

The Grade-Recovery-Performance index is then calculated from the AGR and EGR indices as follows:

$$GRP = \frac{AGR}{|1 - EGR|} \quad (9)$$

A higher GRP index indicates a curve that is located further up and to the right, and well-centred between the two axes. Because the maximum grade or recovery value used for normalization can vary depending on the experimental set being compared, the GRP index in batch operation is a relative measure rather than an absolute one.

2.6.2. Continuous operation

In continuous processes, the GRP index calculation is limited to the plant's final concentrate product. The grades and recoveries are normalized using the theoretical maximum grade $G_{max,th}$ and theoretical maximum recovery $R_{max,th}$. The theoretical maximum recovery is 100 %, while the theoretical maximum grade represents the mass weight of the mineral in all partially and fully liberated particles in the feed ore. For fully liberated particles, the theoretical maximum grade of a mineral is 100 %. The Absolute Grade-Recovery index (AGR) and the Equilibrium Grade-Recovery index (ERG) in continuous operation are calculated as follow:

$$AGR_{Conti} = \left[\left(\frac{R}{R_{max,th}}\right)^2 + \left(\frac{G}{G_{max,th}}\right)^2\right]^{1/2} \quad (10)$$

$$EGR_{Conti} = \frac{R/R_{max,th}}{G/G_{max,th}} = \frac{R^*G_{max,th}}{G^*R_{max,th}} \quad (11)$$

The Absolute Grade-Recovery index is then calculated similarly to the batch mode according to the following equation:

$$GRP = \frac{AGR_{Conti}}{|1 - EGR_{Conti}|} \quad (12)$$

3. Results

3.1. Microflotation

The effect of colloidal silica dosage on the microflotation recoveries of calcite and scheelite is shown in Fig. 6.

It can be seen that colloidal silica depresses calcite, while the recoveries of scheelite are not affected by the reagent, irrespective of its modification. Moreover, the silane modified colloidal silica has the strongest depressing effect on calcite, followed by the non-functionalized and aluminate modified colloidal silica, respectively.

3.2. Batch flotation

In the screening phase, the single parameter effects were evaluated regarding tungsten recovery and the tungsten-calcium selectivity index, as displayed in Fig. 7 **a & b**, respectively. The selectivity index (SI) is calculated according to Gaudin (Gaudin, 1939) using Equation (13); where R_m and R_g are respectively the recoveries of the valuable and gangue minerals.

$$SI = \sqrt{\frac{R_m{}^*(100 - R_g)}{(100 - R_m)^*R_g}} \quad (13)$$

The effect of a parameter is defined as the change in the target variable when the parameter is varied from its lower to its upper level, while

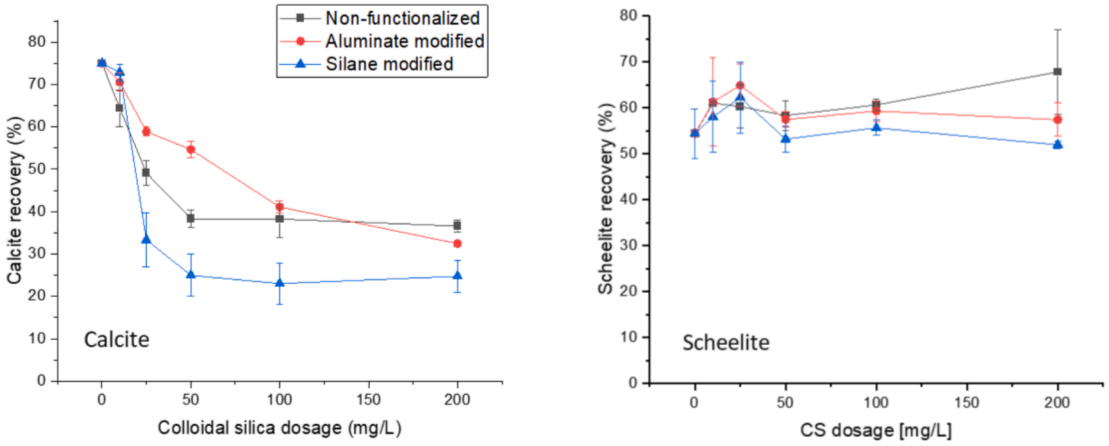


Fig. 6. Single-mineral flotation recoveries of calcite and scheelite depending on colloidal silica dosage (at pH 8, $c_{collector} = 1{\cdot}10^{-3}$ M sodium oleate, colloidal silica specific surface area 500 m^2/g).

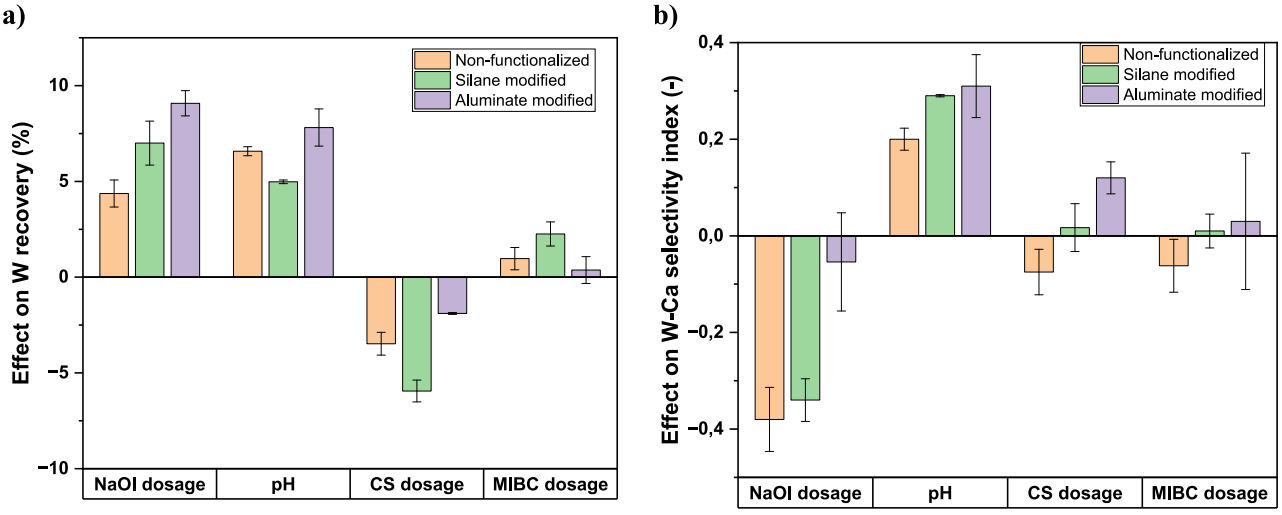


Fig. 7. Absolute effects of the process parameters according to the experimental design in Table 2 on tungsten (W) recovery (a) and tungsten (W) vs. calcium (Ca) selectivity index (b).

keeping all other parameters constant. Mathematically, this is expressed as follow:

$$Effect = \overline{Y}_{A_+} - \overline{Y}_{A_-} \quad (14)$$

Where:

- $\overline{Y}_{A_+}$: average response when A is at the high level
- $\overline{Y}_{A_-}$: average response when A is at the low level

As described in the methodology, the aim of this step is to identify the most important experimental parameters to be further investigated in the investigation and modelling phase, rather than optimize the operating conditions.

The most significant impact on tungsten recovery (Fig. 7**a**) comes from sodium oleate dosage and pH value, irrespective of the colloidal silica modification used. These parameters also significantly influence the scheelite-calcite selectivity index (Fig. 7**b**), which indicates the relevance of investigating these further in the modelling phase. CS dosage negatively impacts scheelite recovery for all three modifications. While this effect is less significant for the tungsten-calcium selectivity index, particularly for the non-functionalized and silane-modified colloidal silica, the colloidal silica dosage is kept as a process parameter and the investigated range is broadened in the modelling phase. Fig. 7 indicates that MIBC dosage has only a minor role in the response variables. This is also confirmed by the significance test as illustrated in tables 15 and 16 in the appendix, where the MIBC dosage parameter is not significant for all response variables at a 95 % confidence interval. Consequently, MIBC dosage is disregarded as a variable in the subsequent phases and set at 0.17 mmol/L.

The decline in scheelite recovery with increasing colloidal silica (CS) dosage beyond a certain threshold was assumed to result from a combination of factors. Initially, the addition of colloidal silica enhances scheelite recovery due to its selective adsorption on calcite, which improves scheelite-calcite selectivity (Ben Said et al., 2024). However, as the colloidal silica dosage increases, its impact on froth properties—such as bubble size and stability—becomes more pronounced, potentially leading to a decline in recovery. At elevated dosages, it is hypothesized that the formation of gel networks or aggregation of colloidal silica could increase pulp viscosity, further reducing recovery by altering bubble-particle interactions and froth drainage behaviour. These combined effects—selective adsorption, froth destabilization, and increased viscosity—are proposed to explain the anticipated trend of an initial increase followed by a decrease in scheelite recovery with rising colloidal silica dosage (Ben Said et al., 2024).

In the investigation and modelling phase, the choice of colloidal

silica dispersion that will be used for pilot and industrial scale depends on two criteria:

i. the effect on the scheelite-calcite selectivity index compared to the blank tests.
ii. and the economic feasibility.

Fig. 8 shows the effect of colloidal silica dosage on the target variable scheelite-calcite selectivity index for the different colloidal silica dispersions. It is clear that the aluminate-modified colloidal silica with a specific surface area of 1100 m^2/g has the most important effect at a dosage of 550 g/t. At the time of this study, this specific reagent is also advantageous in terms of economic feasibility.

The optimal parameter settings for the scheelite-calcite selectivity index for the aluminate-modified colloidal silica with a specific surface area of 1100 m^2/g at batch flotation scale are given in Table 5. These values correspond to an MIBC dosage of 0.17 mmol/L, which was kept fixed in this investigation after the screening phase. As the found optimal parameter settings correspond to a run performed in the experimental plan, no verification is needed.

3.3. Pilot tests

The parameter space investigated with the Nelder Mead method in pilot scale is displayed in Table 6 for both the full and simplified schemes. Assumptions for the selection of variables for the simplified scheme are as follows:

i. Parameters of interest, which will vary widely within the optimization path:
- Colloidal silica dosage: aim of this study and potential new reagent for industrial operations.
- Quebracho dosage: used industrially as a silicate depressant, is known to depress both scheelite and calcite and may interact with the effect of colloidal silica.

ii. Parameters already optimized in batch scale, which will vary only within a minimal range near the optimal value:
- pH,
- collector dosage,
- frother dosage

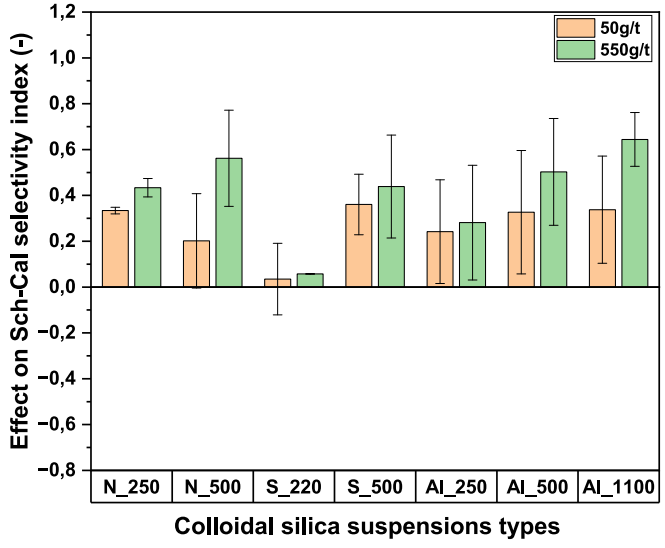


Fig. 8. Effects on scheelite-calcite selectivity index of colloidal silica dosage in comparison to blank tests for seven types of colloidal silica suspensions according to the experimental design in Table 4.

Table 5
Optimal parameter settings of ph, collector dosage and cs dosage for the target variable scheelite-calcite selectivity index for the aluminate-modified colloidal silica with a specific surface area of 1100 m^2/g.

Parameter	pH (−)	Collector dosage (g/t)	CS dosage (g/t)
Optimal setting	10	100	550

These assumptions allow simplifying the starting simplex from 9 to 3 components, which considerably reduces the test workload. If the results obtained with the full and simplified strategies are analogous, there is enough evidence to support the use only of the simplified strategy in the industrial settings. Table 6 summarizes the parameters used for both the full and the simplified schemes, along with the experimental range.

Tables 7 and 8 show the process parameter settings for the full and simplified scheme.

To optimize scheelite-calcite selectivity while maximizing scheelite recovery, the objective was to minimize the target variable, defined as the sum of scheelite recovery in the tailings and calcite recovery in the concentrate. This approach ensures a comprehensive optimization by simultaneously addressing selectivity and recovery.

The algorithm of simplified scheme converged within three iterations reaching a standard deviation of the target variable of 5 %. In contrast, the full scheme was limited to two iterations to serve as a comparative benchmark for the simplified approach. The purpose of the full scheme was to investigate if both schemes move toward the same convergence zone, highlighting the efficiency of the simplified scheme while validating its alignment with the full scheme's behaviour.

The 2D density plot in Fig. 9 shows the convergence zones of the parameters values across the vertices of simplexes produced in the last iteration of the full (**i**) and simplified (**ii**) scheme for pH (**a**), frother and collector dosage (**b**), and colloidal silica and quebracho dosage (**c**). From these plots, it is evident that the parameter values across the vertices converge to the assumed optimal parameter settings derived from batch flotation experiments: [9; 10] for pH, [80; 100] g/t for collector dosage, and [0.10; 0.16] mmol/L for frother dosage. For colloidal silica dosage, the convergence range is between 250 g/t and 450 g/t. In the case of quebracho dosage, the convergence range is between 15 g/t and 25 g/t.

Tables 17 to 23 in the appendix present the vertex parameter values and function evaluations for both the full and simplified schemes. Tables 20 and 23, which display the simplexes produced in the final iterations of the simplified and full schemes, respectively, include the mean values of the parameters across the vertices.

Table 9 illustrates the best performance results for the full and simplified schemes. Almost the same results are obtained with the full and simplified schemes. Consequently, 60 % fewer experiments are performed with the simplified scheme, consuming proportionally less material, energy, and time. Furthermore, the implementation of colloidal silica in the reagent system enhances scheelite-calcite selectivity compared to the benchmark process.

3.4. Industrial trials

A four-day industrial campaign was conducted using the NM simplex method. The process parameters quebracho dosage, collector dosage, and colloidal silica dosage in the rougher and cleaner stages were varied. Both frother dosage and pH were kept constant provided the evidence collected until this point. To evaluate the process performance, the GRP index was implemented. According to the MLA analysis, the scheelite content in all partially and fully liberated particles containing scheelite is 94.23 % corresponding to 75.88 % of WO_3. This would be the theoretical maximum WO_3 grade for the calculation of the GRP index **(cf. 2.6.2)**. The initial simplex is then built from five vertices as described in Table 10. The first vertex represents the reagent dosages of the benchmark process. The second, fourth, and fifth vertices had nearly optimal

Table 6
Process parameter for the full scheme and process parameter varied in the simplified scheme.

Parameter	pH rougher (−)	pH cleaner (−)	Quebracho dosagerougher (g/t)	Collector dosagerougher (g/t)	Collector dosagecleaner (g/t)	Frother dosagerougher (mmol/L)	Frother dosagecleaner (mmol/L)	CS dosagerougher (g/t)	CS dosagecleaner (g/t)
Full scheme	X [8–10]	X	X [0–50]	X [40–150]	X	X [0.059 – 0.32]	X	X [0 – 500]	X
Simplified scheme	[9–10]		X [0 – 30]	[90 – 100]		[0.10 – 0.16]		X [0 – 500]	X

Table 7
Process parameter settings for the start simplex of the full scheme.

Rougher stage					Cleaner stage			
pH (−)	**Quebracho dosage (g/t)**	**Collector dosage (g/t)**	**Frother dosage (mmol/L)**	**CS dosage (g/t)**	**pH (−)**	**Collector dosage (g/t)**	**Frother dosage (mmol/L)**	**CS dosage (g/t)**
9.8	16	30	0.079	0	9	30	0.020	0
8	40	70	0.040	200	9	30	0.079	250
8.5	65	50	0.079	300	8	50	0.079	50
9.2	25	30	0.12	250	10	60	0.040	100
10	30	40	0.059	0	9.2	50	0.079	250
9	0	70	0.099	150	9.5	30	0.040	150
8	50	100	0.12	300	8.6	50	0.20	100
10	10	10	0.020	100	9.8	80	0.079	400
8	35	30	0	100	8.5	10	0.059	100
9	16	30	0.079	0	9.8	30	0.020	150

Table 8
Process parameter settings for the start simplex of the simplified scheme.

Rougher stage					Cleaner stage			
pH (−)	**Quebracho dosage (g/t)**	**Collector dosage (g/t)**	**Frother dosage (mmol/L)**	**CS dosage (g/t)**	**pH (−)**	**Collector dosage (g/t)**	**Frother dosage (mmol/L)**	**CS dosage (g/t)**
9.2	25	30	0.12	250	10	60	0.040	100
10	30	40	0.059	0	9.2	50	0.079	250
9	0	70	0.099	150	9.5	30	0.04	150
10	10	10	0.020	100	9.8	80	0.079	400

parameter settings identified on a pilot scale. The third vertex was set far outside the pre-identified optimal range for the quebracho and collector dosages to ensure the optimization procedure moved in the right direction. These expected results were confirmed in the industrial trials with the lowest GRP index overall (Table 10). Using this strategy assured that the plant operated with recovery losses only during the two hours used for these conditions, guaranteeing the convergence of the simplex in the correct region of the parameter space. Point 3 is then replaced by a reflection point with an improved GRP index. Subsequent reflection, expansion, or contraction points were formed iteratively. The optimization path continued until the termination criterion was met, i.e. until the standard deviation of the GRP indices of the last iteration is smaller than or equal to 5 %, which occurred after 5 iterations. Fig. 10 shows the optimization path of the simplex through the formation of reflection and expansion points until it converged. The parameter settings of the vertex with the optimal parameter settings are described in Table 11. At the optimum conditions, the WO_3 grade was 13 % higher than the benchmark, representing an improvement ratio of 42 %, while the recovery increased by approx. 2.5 % (Fig. 11).

4. Effect of ore variability and statistical significance of the performed industrial trials

After performing the optimization trials, a short production downtime took place where extraction activities were carried out. Using the optimal parameters of the optimum trial, a longer trial lasting 4 h was conducted after the extraction activities, namely the validation trial. Fig. 12 shows the scheelite and calcite grades in the feed and concentrate of the benchmark, optimum, and validation trials. The results suggest an improvement in the scheelite grade of the very last cleaner concentrate by 12 % and a decrease in the calcite grade by 7 % for the trial before the extraction activities. Yet, these results could not be replicated in the 4 h trial, which achieved an increase of 7 % in scheelite grade and an increase of 1 % in calcite grade. Such variations could be caused by a significant difference in ore properties between the material being processed before and after the extraction activities. MLA measurements were thus performed for the feed and cleaner-4-concentrate of the benchmark (It0_P1_Benchmark), optimal (It3_Xr_Optimum), and validation trials (Optimum_4h).

Fig. 13 shows the size distribution of calcite mass according to particle size class for the different feed and concentrate samples. The particle size fraction < 115 μm constitutes 55 % of all calcite mass in the feed of the validation trial. In contrast, this fraction makes up 70 % of the feed of the other two trials. Given that calcite particles in the < 115 μm size fraction accounts for more than 95 % of the total calcite mass in the concentrates, and that the calcite grades in the feeds are almost the same (Fig. 12 **b**), calcite microstructures variations in the validation trial are responsible for the decrease in recovery observed. On the other hand, calcite grade in the concentrate is higher for the validation trial than for the optimization trial. This variation could be caused by the flotation behaviour of other gangue minerals in the ore.

Fig. 14 **a** shows the mineralogical composition of the different concentrates. Besides scheelite and calcite grades, the main differences in the concentrates' mineralogical compositions between the optimization

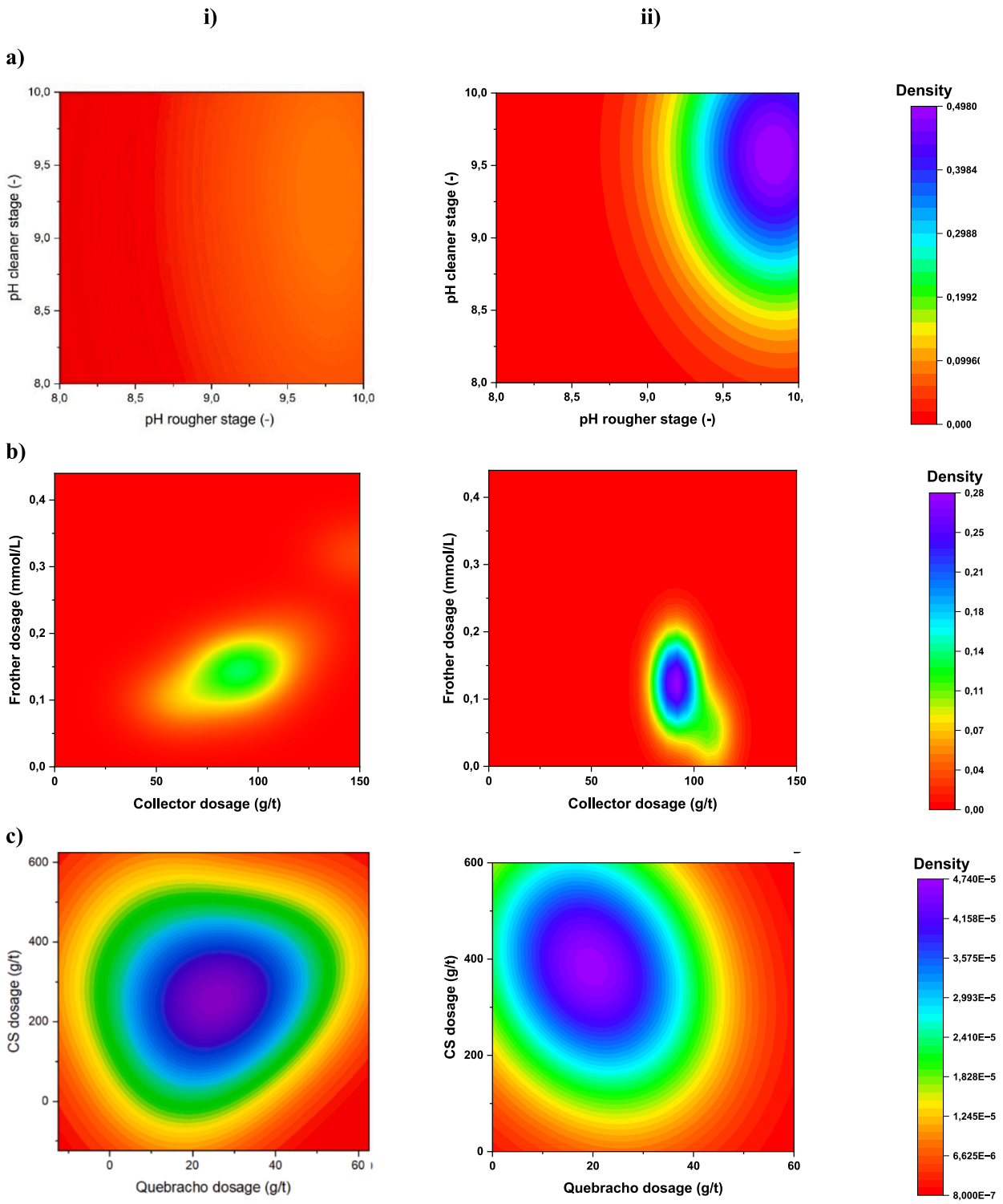


Fig. 9. 2D representations of the density of simplex points of the third iteration of the full (i) and simplified (ii) scheme for the process variables pH value (a) collector and frother dosages (b) and quebracho and colloidal silica dosages (c).

and validation trials is observed for talc grades. These are significantly lower between the benchmark and both trials where colloidal silica is used (Fig. 14 **b).** Talc, known for its high hydrophobicity (Ann Bazar et al., 2021), was not significantly present in the batch flotation experiments, but is an important gangue mineral for the industrial trials.

The particle size distribution of talc in the feed and concentrate samples of the different trials are shown in Fig. 15. A significant difference in the fraction of fine talc particles between the optimization trials before and after the extraction activities is observed. For the optimum trial, 90 % of the talc particles are smaller than 115 μm, whereas in the validation trial, only approx. 75 % of the particles fall within this range. Given that this particle size fraction constitutes 98 % of the talc particles present in the concentrates, and the similar talc feed grades (Fig. 16), talc microstructure properties might be responsible for their lower recovery in the validation trial. Consequently, this would explain the higher calcite grade in the concentrate of the validation trial.

Table 9
Comparison between the results of the benchmark process and the optimal parameter settings achieved after three four iterations for the full and the simplified schemes.

	pH rougher [-]	pH cleaner [-]	Sum collector dosage (g/t)	Sum frother dosage (mmol/L)	Quebracho dosage rougher (g/t)	Sum CS dosage (g/t)	Scheelite grade (%)	Scheelite recovery (%)	Calcite recovery (%)
Benchmark	9.8	9	60	0.10	16	0	4.38	84.36	25.84
Full scheme	10	9.24	116	0.19	21	315	8.11	75.95	7.06
Simplified scheme	9.55	9.65	92	0.13	17	350	7.11	74.09	11.01
Simplified scheme to benchmark							+2.73	−10.27	−15.83
Simplified to full scheme							−1.00	−1.86	+2.95

Table 10
Parameter settings of the start simplex of the industrial trials.

Iteration 0 – Start Simplex				Results		
Quebracho dosage	Collector dosage	CS dosage Rougher stage	CS dosage Cleaner stage	WO_3grade	WO_3recovery	GRP-Index
(g/t)	(g/t)	(g/t)	(g/t)	(%)	(%)	(−)
16	60	0	0	29.40	85.46	0.78
20	80	0	250	37.63	86.31	1.34
8	40	250	0	25.78	83.46	0.62
22	100	125	125	38.99	87.15	1.45
5	110	180	70	26.84	86.92	0.64

Interpreting the results from a recovery perspective and linking them to ore variability and reagent system effects would provide more insights and allow for more meaningful conclusions. Due to technical limitations, only data about scheelite recovery are available. Nevertheless, these observations underline the importance of considering the system as a whole, paying specific attention to minerals that could compete with the minerals of interest and affect the flotation efficiency of the target minerals, as talc does in this study. The effect of ore variability on the performance of the flotation process has already been highlighted in many studies e.g. (Tijsseling et al., 2020). This implies that the developed methodology should be extended to address the issue of feed variability in its framework — starting from laboratory scale. This could be achieved, for example, by identifying minerals that can compete with the flotation of minerals of interest early on to include these in the preliminary studies. In the context of geometallurgy, this could be accomplished by conducting an experimental campaign on samples collected in locations of expected variations in microstructure of the orebody. Later, ore microstructures could then be incorporated in the optimization routine, for example with a link to particle-based separation modelling approaches (Deng et al., 2018).

It is well known that the feed ore grade has a big impact in the shape of the grade recovery curve (Drzymala et al., 2013). Higher feed ore grades tend to result in steeper grade-recovery curves, as the increased presence of valuable minerals allows for higher concentrate grades without significant drops in recovery. Conversely, lower feed grades often lead to flatter curves, where high recoveries can still be reached but at lower concentrate grades. Essentially, feed ore grade variability influences the balance between these two dimensions. Fig. 17 illustrates the relationship between the GRP index, along with its sub-indices AGR and EGR indices, and the feed ore grade. The AGR index shows considerably lower sensitivity compared to both the EGR and GRP indices, as confirmed by the descriptive statistics in Table 12.

This reduced sensitivity of the AGR index can be explained by its design, which aims to capture overall process performance across both grade and recovery, without being overly influenced by either metric. As a result, the AGR index is less affected by changes in feed ore grade. On the other hand, the EGR index, which emphasizes how much the process outcome leans toward one of the two dimensions (grade or recovery), exhibits higher sensitivity to variations in feed ore grade. Therefore, the GRP index not only offers a comprehensive metric for evaluating process performance across both dimensions, but its sub-indices also allow for targeted assessment of the process with varying degrees of sensitivity to feed ore grade. Nonetheless, this finding warrants further investigation, particularly under conditions of greater feed ore grade variation and for different systems.

To evaluate the statistical significance of the impact of implementing colloidal silica in the reagent system on process performance, data from the week before implementation, provided by the Advanced Process Control System at the industrial plant, was compared with data from the week during the optimization trials. The collected data underwent a cleaning process to remove values outside of stable production conditions. Specifically, data from the beginning of production and during production downtime were excluded, ensuring only data from stable production periods were retained. This cleaning involved filtering based on other measured plant parameters, such as ball mill output and pH values, which were maintained within a constant range.

Table 13 presents key descriptive statistics from the datasets for the week before and the week during the optimization trials, with their distribution is illustrated in the box plots in Fig. 18. The red points represent the grades from the final simplex (Iteration 5) of the optimization path, with the star indicating the WO_3 grade achieved using the optimal parameter settings. It is evident that the optimization trial results extend beyond the typical range shown in the boxplots, with four data points from the week prior to the trials exceeding the 99th percentile. Despite the large datasets, a more comprehensive statistical analysis requires a longer testing period spanning weeks or months. This should involve alternating between the use of colloidal silica in the reagent system and its absence to thoroughly assess the impact.

The Combination of statistical design of experiments and NM optimization used in this study and simplifying the algorithm based on batch flotation results aligns with the proposed modifications to improve convergence. The strongest point of this combination is its ability to bridge the gap between batch and continuous operations in batch flotation and reduce uncertainties caused by differences in operation modes. Constraining the optimization algorithm by predefining optimal parameter settings at lab scale and building the start simplexes for the NM algorithm around them may push the algorithm to converge in a certain region, potentially trapping it in a local optimum, which may not be the global optimum for continuous industrial operations. However, in industrial settings, finding a local optimum is often sufficient. Engineers

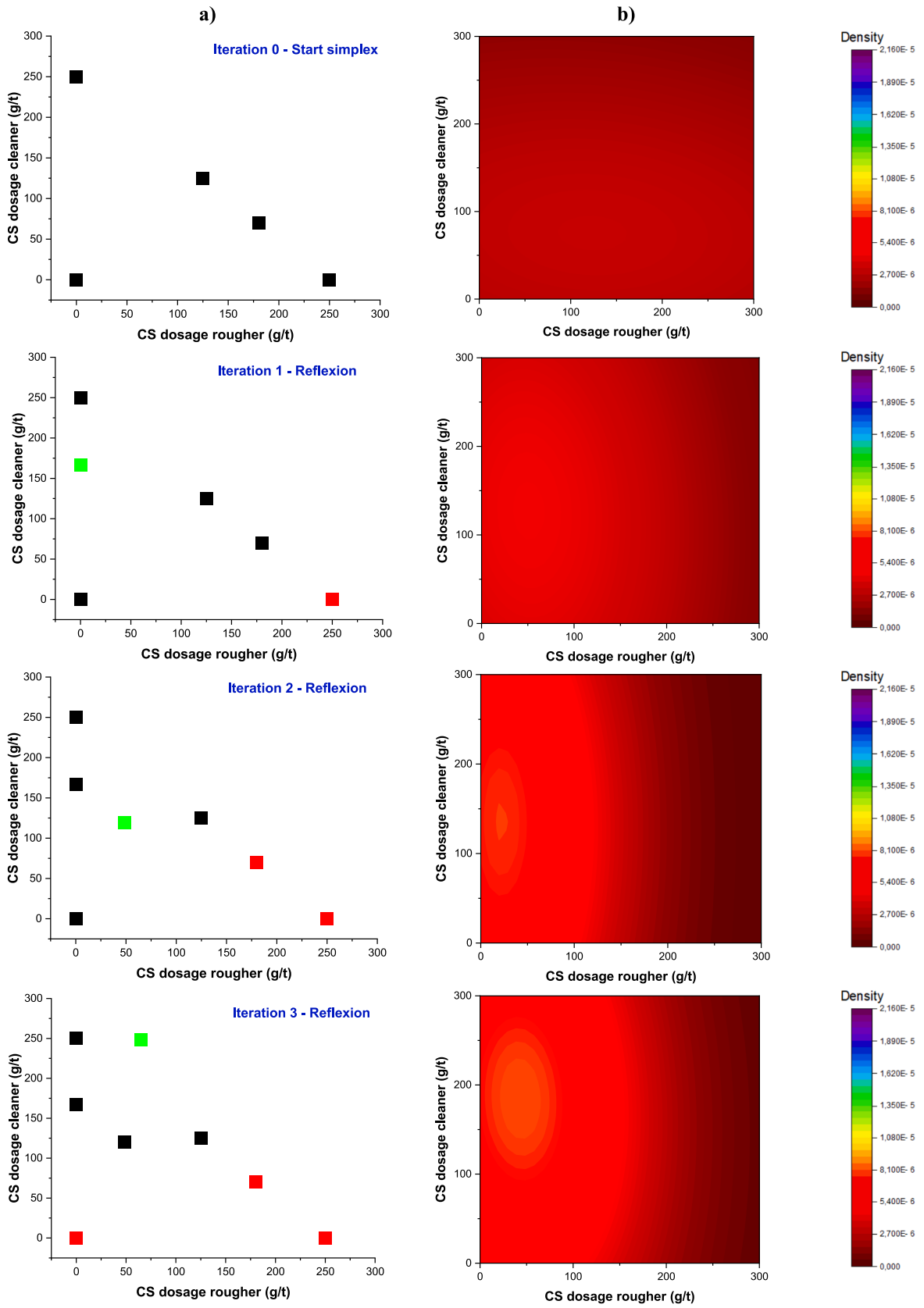


Fig. 10. Two-dimensional dot diagram (a) and density diagram (b) illustrate the simplexes for different iterations of the optimization path for colloidal silica dosages in the rougher and cleaner stages. The reflection points are coloured light green. Expansion points are coloured orange. Points that drop from the simplexes are shown in red. The points used to calculate the reflection/expansion points are marked in black.

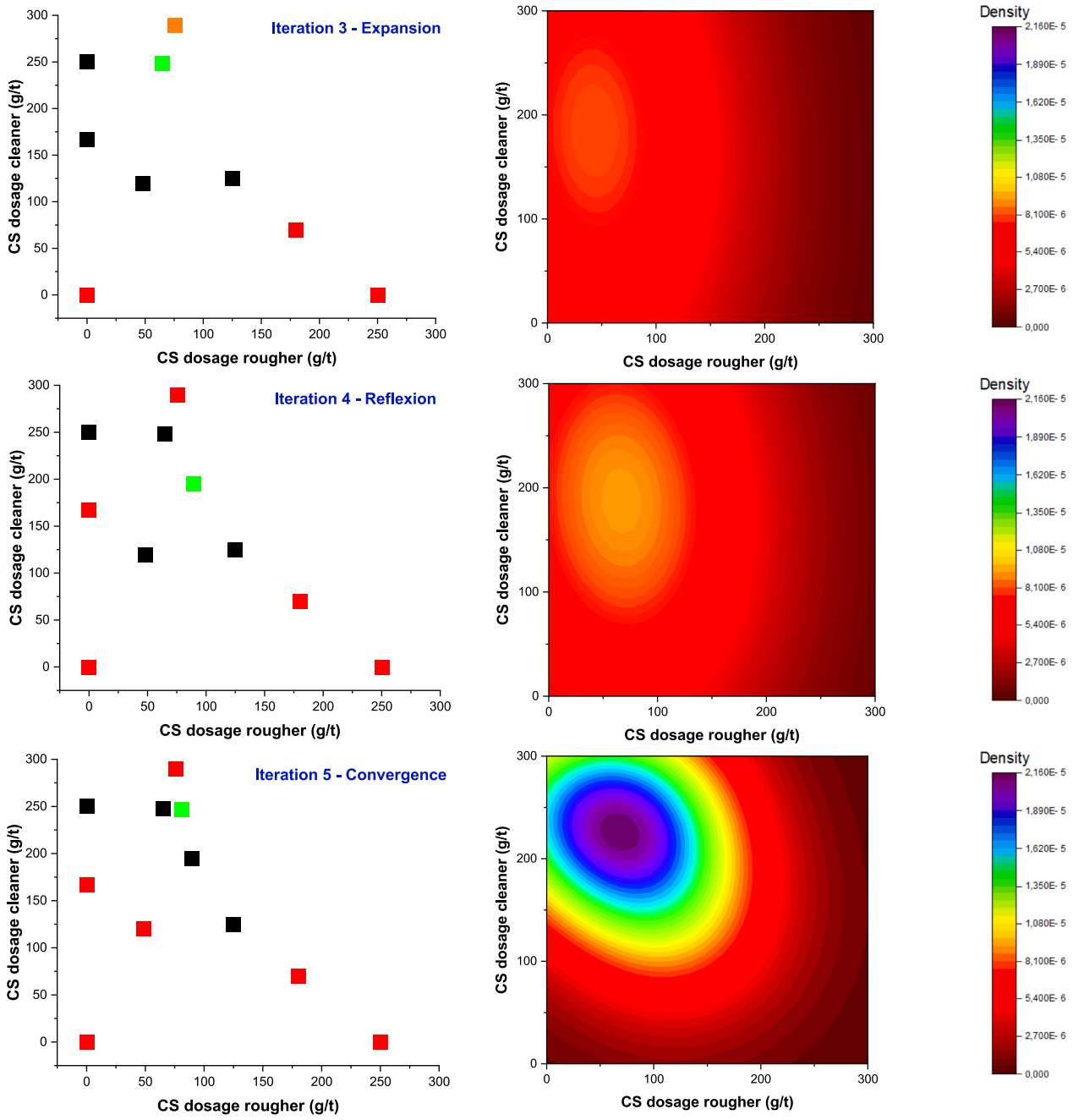


Fig. 10. (*continued*).

Table 11
Parameter settings of the vertex with the optimal parameter settings of the industrial trials.

Iteration 5 – Optimal parameter settings				Results		
Quebracho dosage	Collector dosage	CS dosage Rougher stage	CS dosage Cleaner stage	WO_3grade	WO_3recovery	GRP-Index
(g/t)	(g/t)	(g/t)	(g/t)	(%)	(%)	(–)
22	108	65	248	41.95	88.49	1.74

and plant operators typically prioritize stability and reliability over the theoretical best solution, as maintaining optimal conditions and a stable plant is crucial for continuous operations. Finding the global optimum can be computationally expensive and time-consuming, and the effort and cost involved may not justify the marginal performance gains.

Our approach, which integrates Design of Experiments (DoE) and numerical optimization across lab, pilot, and industrial-scale experiments, offers significant advantages over traditional simulation-based methods. It effectively bridges the gap between batch and continuous operations, reducing uncertainties arising from operational differences while minimizing the reliance on extensive computational resources. Traditional simulations often fail to adequately capture operational

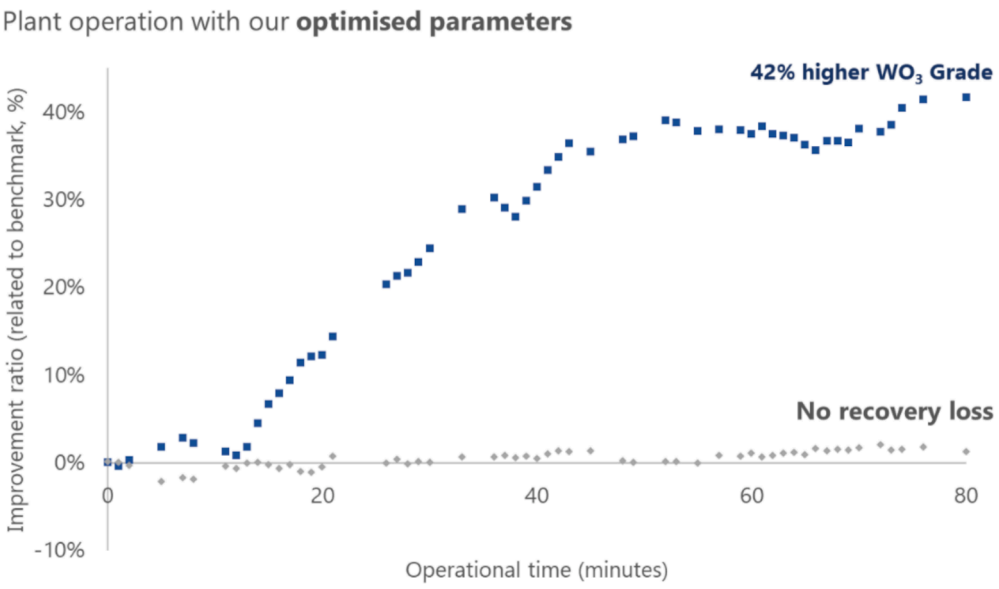


Fig. 11. The improvement in KPIs of scheelite grade and recovery during the industrial trial with optimal parameter settings.

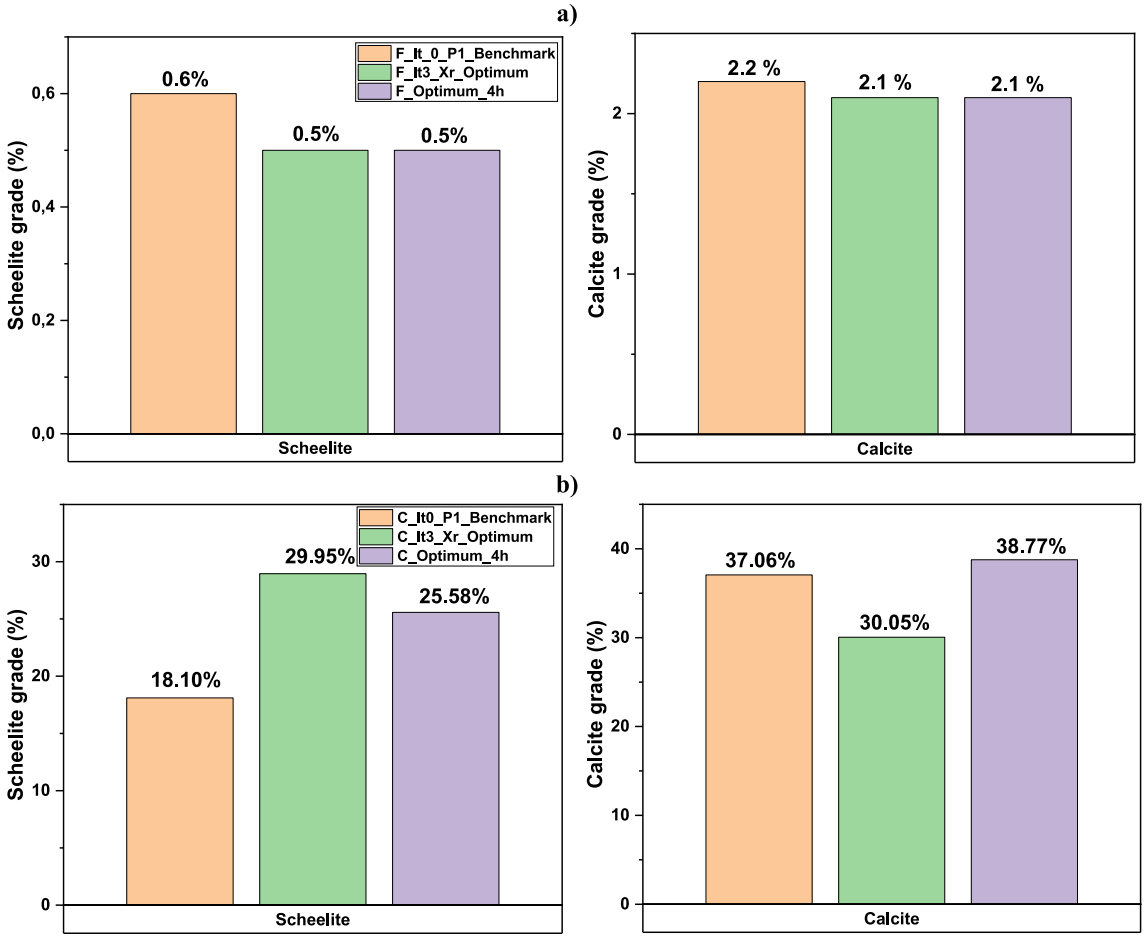


Fig. 12. Scheelite and calcite grades in the feed ore (a) and the concentrates of the before last cleaner (b) of the benchmark process (C_It0_P1_Benchmark), the optimal trial found in the optimization procedure (C_It3_Xr_Optimum), and the 4 h trial after the extraction activities (C_Optimum_4h).

variability, necessitating plant-scale validation to verify their predictions. Simulations rely on assumptions that may not align with real-world conditions and require detailed size-by-mineral data for each separation stage—data that is often difficult to obtain. Additionally, developing and calibrating models for complex processes is both computationally intensive and demands specialized expertise (Erkan et al., 2022). Our approach addresses these challenges by minimizing assumptions and ensuring practical applicability in industrial settings.

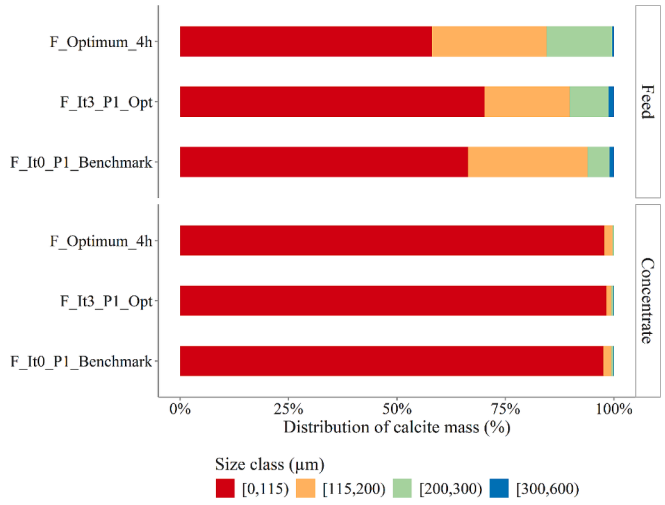


Fig. 13. Distribution of calcite mass across particle size classes in the feed and concentrates of the benchmark (It0_P1_Benchmark), the optimal (It3_Xr_Optimum), and validation (Optimum_4h) trials.

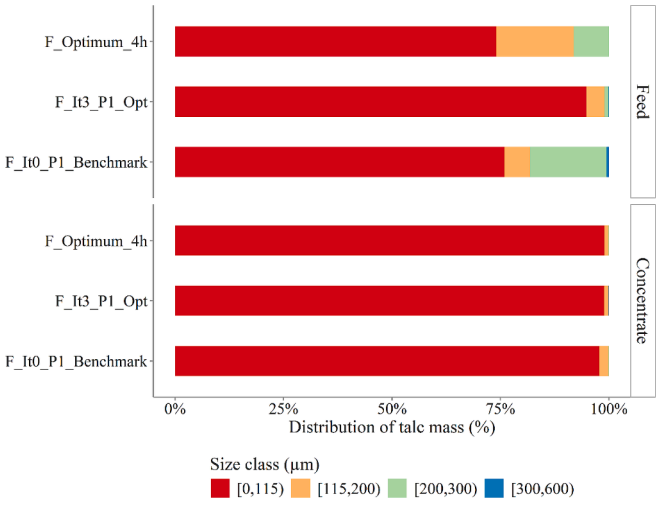


Fig. 15. Distribution of talc mass across particle size classes in the feed and concentrates of the benchmark (It0_P1_Benchmark), the optimal (It3_Xr_Optimum), and validation (Optimum_4h) trials.

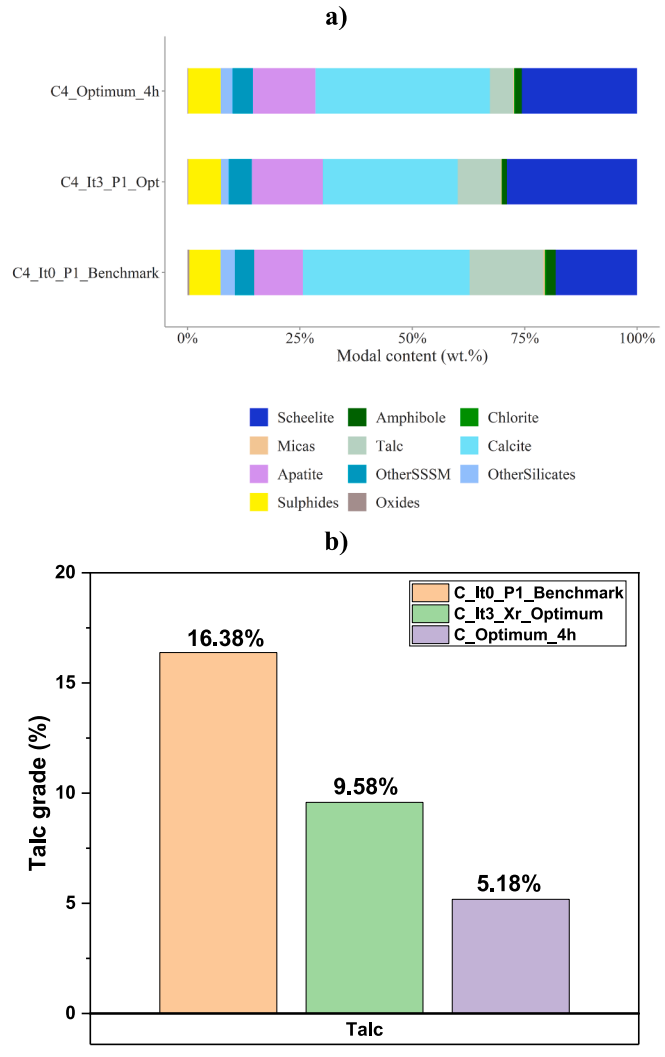


Fig. 14. Modal Mineralogy of the concentrates (a) and talc grade (b) of the benchmark process (It0_P1_Benchmark), the optimal trial found in the optimization procedure (It3_Xr_Optimum), and the 4 h trial after the extraction activities (Optimum_4h).

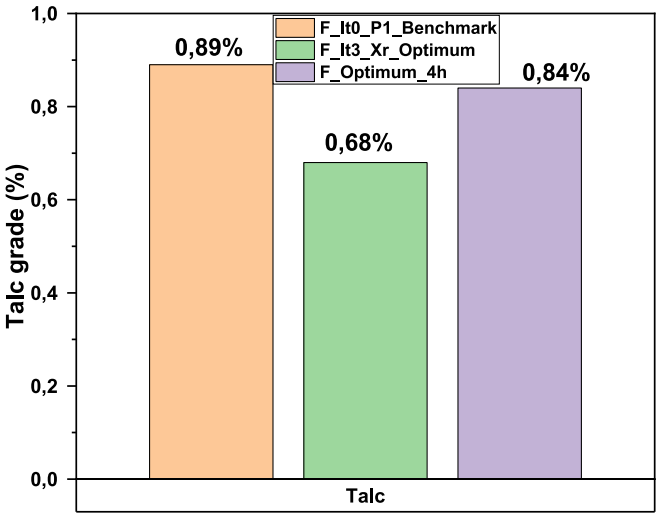


Fig. 16. Talc grades in the feed ores of the benchmark process (F_It0_P1_Benchmark), the optimal trial found in the optimization procedure (F_It3_Xr_Optimum), and the 4 h trial after the extraction activities (F_Optimum_4h).

Data-Driven Model Predictive Control (MPC) uses a dynamic model based on a Gate Recurrent Unit (GRU) network and an optimizer to guide reagent addition in tungsten flotation. It aims to accurately predict concentrate grade and optimize the reagent addition process (Wan et al., 2021). Deep learning integrated with the likelihood function has been used to predict clean coal ash content, considering froth velocity and reagent dosage parameters (Lu et al., 2023). Nuorivaara et al. (Nuorivaara et al., 2019) developed a strategy to reduce flotation reagent and fresh water consumption by optimizing conditioning parameters and implementing water recycling initiatives. This minimizes additional resource expenses while maintaining flotation performance. Similarly, a Framework for Reagent Selection proposed by Stanujkić et al. (Stanujkić et al., 2017) aids in selecting the most appropriate flotation reagents. It considers unique ore characteristics across various mine sites, using methodologies like SWARA and WS-PLP to evaluate and select reagents.

The proposed methodology is well-suited for integration with process control technologies, which are designed to fine-tune processing plants during operation, such as by compensating for real-time

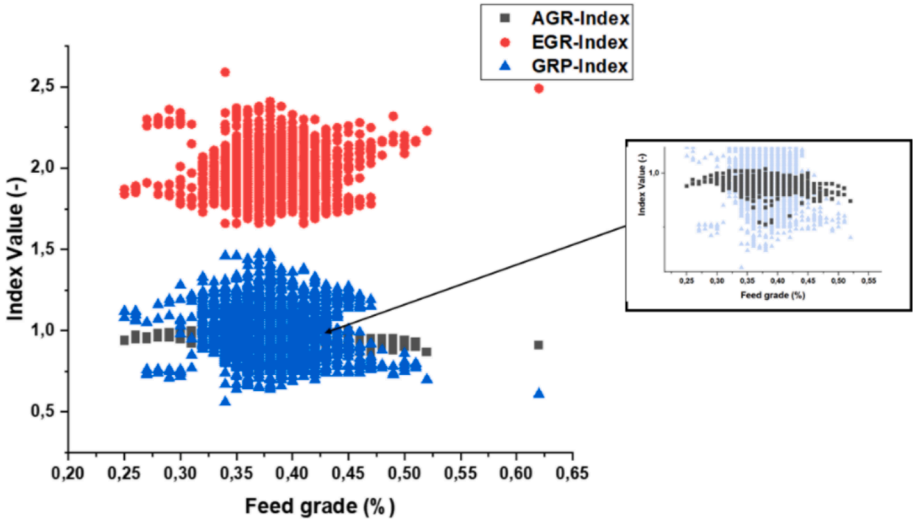


Fig. 17. Relationship between the GRP index, along with its sub-indices AGR and EGR, and the feed ore grade. for the week before the optimization trials.

Table 12
Descriptive statistics of the datasets of the feed ore grade and the different indices for the week before the optimization trials.

	Mean	Standard Deviation	Minimum	Median	Maximun
Feed grade (%)	0.37	0.035	0.25	0.037	0.62
AGR-Index (—)	0.95	0.023	0.76	0.95	1.02
EGR-Index (—)	1.98	0.13	1.66	1.98	2.59
GRP-Index (—)	0.98	0.14	0.56	0.97	1.47

variations in feed ore composition. Various strategies for controlling and optimizing established reagent systems in industrial-scale froth flotation have been developed. Lu et al. (Lu et al., 2022) proposed a Two-Step Optimal-Setting Control combining a basic dosage pre-set model with a feedback reagent addition compensation model. They used the belief rule base (BRB) method and the state transition algorithm (STA) to optimize model parameters and refine automatic reagent addition. Other methods to improve flotation performance include reagent dosage control based on bubble size characteristics (Xie et al., 2016),and a Hybrid Model for Switching and Optimizing Control (Dong et al., 2017). The latter combines froth depth fuzzy control with an expert system for reagent dosage optimization, employing wavelet analysis, principal component analysis (PCA), and the least squares-support vector machine (LS-SVM) to identify optimal operating conditions and enhance the flotation process. Our approach is well-designed to integrate these advancements, leveraging data-driven and optimization techniques to improve flotation efficiency and resource utilization.

5. Conclusion

This study presents a novel approach that integrates the statistical design of experiments with NM optimization, streamlining the algorithm based on batch flotation outcomes. This method improves convergence by bridging the gap between batch and continuous operations in flotation processes, reducing uncertainties from different operational modes. The proposed workflow minimizes the risk of plant-damaging trials by identifying optimal conditions at the pilot scale before industrial testing. Conducting most of the work at laboratory and pilot scales saves both time and resources, avoiding prolonged and unsystematic industrial trials. The developed GRP-Index was successfully applied at the industrial scale, providing a quantitative tool to evaluate plant performance in terms of valuable mineral grade and recovery. The study also reaffirmed the impact of ore variability on flotation performance. For example, a shift in the particle size distribution of the highly hydrophobic gangue mineral, talc, reduced the negative impact of colloidal silica on calcite grade in the concentrate. This suggests the developed methodology should be expanded to address feed variability, starting at the laboratory scale with a focus on problematic gangue minerals like talc. It is crucial to consider the system as a whole, not just the target minerals during lab-scale studies, to develop strategies for managing ore variability in terms of grade, particle size, liberation, and other relevant properties. Finally, while extensive datasets were analysed during industrial tests to demonstrate the significance of implementing colloidal silica in plant performance, a more comprehensive statistical analysis requires a longer testing period, potentially spanning several weeks or months. This should include alternating between the use of colloidal silica in the reagent system and its absence to thoroughly evaluate its impact.

Table 13
Descriptive statistics of the datasets of WO_3 grade (in %) for the week before and the week during the optimization trials.

N total	Mean	Standard Deviation	Minimum	1 st Quartile (Q1)	Median	2 nd Quartile (Q3)	Maximum	P90	P95	P99
Week before the optimization trials										
2552	32.58	2.08	24.5	31.27	32.53	34.06	38.36	35.25	35.93	37.30
Week of the optimization trials										
3208	31.93	3.47	18.52	29.72	31.72	33.98	42.78	36.56	38.01	40.78

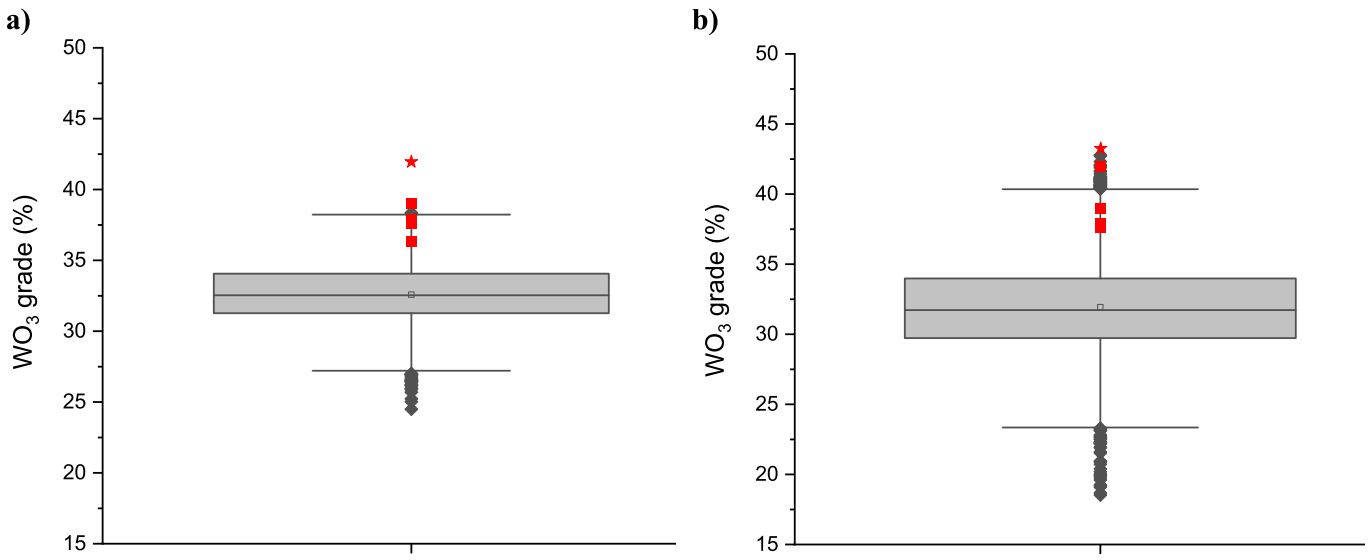


Fig. 18. Box plots of theWO_3 grades for the weeks before the industrial trials (a), and the week during which the trials were conducted (b). WO_3 grades of the last simplex (Iteration 5) in the optimization path are coloured in red. The point marked with a star symbol represents the WO_3 grade with the optimal parameter settings.

CRediT authorship contribution statement

B. Ben Said: Writing – review & editing, Writing – original draft, Validation, Methodology, Investigation, Data curation, Conceptualization. **M. Rudolph:** Writing – review & editing, Supervision, Project administration, Funding acquisition, Data curation. **D. Goldmann:** Writing – review & editing, Supervision. **L. Pereira:** Writing – review & editing, Supervision, Data curation.

Declaration of competing interest

The authors declare that they have no known competing financial interests or personal relationships that could have appeared to influence the work reported in this paper.

Acknowledgements

The authors would like to thank colleagues at Nouryon (formerly AkzoNobel Surface Chemistry, Sweden) for providing flotation reagents and meaningful discussions. The authors would like to thank many colleagues for their support with this project: Roland Würkert for sample preparation and Dr. Bradley Martin Guy for conducting the MLA analyses as well as Dr Robert Möckel and Doreen Ebert for conducting XRD analyses. This paper was written thanks to the financial support of the CoSilFlot project financed by the "WIPANO – Knowledge and Technology Transfer through Patents and Standards" program of the German Federal Ministry of Economic Affairs and Climate Action (BMWK) under funding number 03THWSN006.

Appendix A

Table 14
Estimation of coefficients and effects analysis for the response tungsten recovery. *** Significant to 0.1 %, ** Significant to 1 %, * Significant to 5 %, NS: not significant.

Parameter	Effect	P-value
Non-functionalized		
NaOl dosage	4.37	0.011 *
pH	6.58	0.00078 ***
CS dosage	−3.48	0.033*
MIBC dosage	0.97	0.51 ^{NS}
Silane modified		
NaOl dosage	7.00	0.011 *
pH	4.98	0.053 ^{NS}
CS dosage	−5.94	0.025 *
MIBC dosage	2.26	0.35 ^{NS}
Aluminate modified		
NaOl dosage	9.08	0.00040 ***
pH	7.81	0.0012 **
CS dosage	−1.89	0.31 ^{NS}
MIBC dosage	0.37	0.84 ^{NS}

Table 15
Estimation of coefficients and effects analysis for the response tungsten-calcium selectivity index. *** Significant to 0.1 %, ** Significant to 1 %, * Significant to 5 %, NS: not significant.

Parameter	Effect	P-value
Non-functionalized		
NaOl dosage	−0.38	0.0021 **
pH	0.20	0.061 NS
CS dosage	−0.075	0.44 NS
MIBC dosage	−0.062	0.52 NS
Silane modified		
NaOl dosage	−0.34	0.11 NS
pH	−0.29	0.18 NS
CS dosage	0.017	0.93 NS
MIBC dosage	0.10	0.60 NS
Aluminate modified		
NaOl dosage	−0.054	0.59 NS
pH	0.31	0.0080 **
CS dosage	0.12	0.24 NS
MIBC dosage	0.030	0.76 NS

Table 16
Vertices parameter values, function evaluations, and transformation calculations for Iteration 1 of the simplified scheme.

It.	Point	pH rougher [-]	pH cleaner [-]	Quebracho dosage (g/t)	Collector dosage rougher (g/t)	Collecor dosage cleaner (g/t)	Frother dosage rougher (mmol/L)	Frother dosage cleaner (mmol/L)	CS dosage rougher (g/t)	CS dosage cleaner (g/t)	Sum collector dosage (g/t)	Sum frother dosage (mmol/L)	Sum CS dosage (g/t)	Scheelite recovery (%)	Calcite recovery (%)	$Sch_{rec,Tails} + Cal_{rec,Conc}$(%)	Mean (%)	Std (%)
1	**a**	9.20	10.00	25	30	60	0.12	0.040	250	100	90	0.16	350	75.43	34.94	59.51	56.85	12.85
	b	10.00	9.24	30	40	50	0.059	0.079	0	250	90	0.14	250	65.73	15.39	49.66		
	c	9.00	9.50	0	70	30	0.099	0.040	150	150	100	0.14	300	57.21	30.92	73.72		
	d	10.00	9.87	10	10	80	0.020	0.079	100	400	90	0.099	500	83.47	28.00	44.52		
Centroid of all points except c, which has the highest function value																		
x_c		9.73	9.70	21.67	26.67	63.33	0.066	0.066	116.67	250	90	0.13	366.67					
Reflexion of c through the centroid																		
$x_{r,1}$		10.10	9.80	32.50	5	80	0.050	0.079	100	300	85	0.13	400	34.94	5.79	70.85		
$f(d) < f(x_{r,1}) < f(c)$**: Outside Contraction**																		
$x_{oc,1}$		9.92	9.75	27.08	15.83	71.67	0.058	0.073	108.33	275	87.50	0.13	383.33	51.73	12.04	60.31		
Next		**Replacement of** c **by** $x_{oc,1}$																

Table 17
Vertices parameter values, function evaluations, and transformation calculations for Iteration 2 of the simplified scheme.

It.	Point	pH rougher [-]	pH cleaner [-]	Quebracho dosage (g/t)	Collector dosage rougher (g/t)	Collecor dosage cleaner (g/t)	Frother dosage rougher (mmol/L)	Frother dosage cleaner (mmol/L)	CS dosage rougher (g/t)	CS dosage cleaner (g/t)	Sum collector dosage (g/t)	Sum frother dosage (mmol/L)	Sum CS dosage (g/t)	Scheelite recovery (%)	Calcite recovery (%)	$Sch_{rec,Tails} + Cal_{rec,Conc}$(%)	Mean (%)	Std (%)
2	**a**	9.20	10.00	25.00	30.00	60.00	0.12	0.040	250.00	100	90.00	0.16	350.00	75.43	34.94	59.51	53.50	7.70
	b	10.00	9.24	30.00	40.00	50.00	0.059	0.079	0	250	90.00	0.14	250.00	65.73	15.39	49.66		
	$x_{oc,1}$	9.92	9.75	27.08	15.83	71.67	0.058	0.073	108.33	275	87.50	0.13	383.33	51.73	12.04	60.31		
	d	10.00	9.87	10.00	10.00	80.00	0.020	0.079	100.00	400	90.00	0.10	500.00	83.47	28.00	44.52		
Centroid of all points except $x_{oc,1}$**, which has the highest function value.**																		
x_c		9.73	9.70	21.67	26.67	63.33	0.066	0.066	116.67	250	90	0.13	366.67					
Reflexion of $x_{oc,1}$ **through the centroid**																		
$x_{r,2}$		9.55	9.65	16.25	37.50	55.00	0.070	0.063	125.00	225.00	92.50	0.13	350.00	74.09	11.01	36.92		
Expansion from x_c **through** $x_{r,2}$																		
$x_{e,1}$		9.59	9.67	17.60	34.79	57.08	0.072	0.061	122.92	231.25	91.88	0.13	354.17	69.43	12.67	43.24		
Next		$f(x_{e,1}) > f(x_{r,2})$**: Replacement of** $x_{oc,1}$ **by** $x_{r,2}$																

Table 18
Vertices parameter values, function evaluations, and transformation calculations for Iteration 3 of the simplified scheme.

It.	Point	pH rougher [-]	pH cleaner [-]	Quebracho dosage (g/t)	Collector dosage rougher (g/t)	Collecor dosage cleaner (g/t)	Frother dosage rougher (mmol/L)	Frother dosage cleaner (mmol/L)	CS dosage rougher (g/t)	CS dosage cleaner (g/t)	Sum collector dosage (g/t)	Sum frother dosage (mmol/L)	Sum CS dosage (g/t)	Scheelite recovery (%)	Calcite recovery (%)	$Sch_{rec,Tails} + Cal_{rec,Conc}$(%)	Mean (%)	Std (%)
3	a	9.20	10.00	25.00	30.00	60	0.12	0.040	250	100	90.00	0.16	350	75.43	34.94	59.51	47.65	9.48
	b	10.00	9.24	30.00	40.00	50	0.059	0.079	0	250	90.00	0.14	250	65.73	15.39	49.66		
	$x_{r,2}$	9.55	9.65	16.25	37.50	55	0.070	0.063	125	225	92.50	0.13	350	74.09	11.01	36.92		
	d	10.00	9.87	10.00	10.00	80	0.020	0.079	100	400	90.00	0.10	500	83.47	28.00	44.52		
Centroid of all points except a, which has the highest target function value.																		
x_c		9.85	9.59	18.75	29.17	61.67	0.050	0.074	75.00	291.67	90.83	0.12	366.67					
Reflexion of a through the centroid																		
$x_{r,3}$		10.18	9.38	23.13	31.25	77.50	0	0.051	107.50	312.50	108.75	0.051	420.00	76.38	24.51	48.13		
Next		$f(x_{r,2}) < f(x_{r,3}) < f(b)$**: Replacement of a by** $x_{r,3}$																

Table 19
Vertices parameter values, function evaluations, and transformation calculations for the converged Simplex of the simplified scheme.

It.	Point	pH rougher [-]	pH cleaner [-]	Quebracho dosage (g/t)	Collector dosage rougher (g/t)	Collecor dosage cleaner (g/t)	Frother dosage rougher (mmol/L)	Frother dosage cleaner (mmol/L)	CS dosage rougher (g/t)	CS dosage cleaner (g/t)	Sum collector dosage (g/t)	Sum frother dosage (mmol/L)	Sum CS dosage (g/t)	Scheelite recovery (%)	Calcite recovery (%)	$Sch_{rec,Tails} + Cal_{rec,Conc}$(%)	Mean (%)	Std (%)
3	$x_{r,3}$	10.18	9.38	23.13	31.25	77.50	0	0.051	107.50	312.50	108.75	0.051	420	76.38	24.51	48.13	44.81	5.68
	b	10.00	9.24	30.00	40.00	50.00	0.059	0.079	0.00	250.00	90.00	0.14	250	65.73	15.39	49.66		
	$x_{r,1}$	9.55	9.65	16.25	37.50	55.00	0.070	0.063	125.00	225.00	92.50	0.13	350	74.09	11.01	39.92		
	d	10.00	9.87	10.00	10.00	80.00	0.020	0.079	100.00	400.00	90.00	0.10	500	83.47	28.00	44.52		
Mean of the parameter values		9.93	9.54	19.84	29.69	65.63	0.038	0.067	83.13	296.88	95.31	0.11	380					

Table 20
Vertices parameter values, function evaluations, and transformation calculations for Iteration 1 of the full scheme.

It.	Point	pH rougher [-]	pH cleaner [-]	Quebracho dosage (g/t)	Collector dosage rougher (g/t)	Collecor dosage cleaner (g/t)	Frother dosage rougher (mmol/L)	Frother dosage cleaner (mmol/L)	CS dosage rougher (g/t)	CS dosage cleaner (g/t)	Sum collector dosage (g/t)	Sum frother dosage (mmol/L)	Sum CS dosage (g/t)	Scheelite recovery (%)	Calcite recovery (%)	$Sch_{rec,Tails} + Cal_{rec,Conc}$(%)	Mean (%)	Std (%)
1	a	9.80	8.80	16	30	30	0.079	0.020	0	0	60	0.10	0	84.36	25.84	41.48	65.44	21.95
	b	8.00	9.00	40	70	30	0.040	0.079	200	250	100	0.12	450	2.90	0.02	97.12		
	c	10.00	10.00	65	50	50	0.079	0.079	300	50	100	0.16	350	14.20	3.07	86.87		
	d	9.20	10.00	25	30	60	0.12	0.040	250	100	90	0.16	350	75.43	34.94	59.51		
	e	10.00	9.20	30	40	50	0.059	0.079	0	250	90	0.14	250	65.73	15.39	49.66		
	f	9.00	9.500	0	70	30	0.099	0.040	150	150	100	0.14	300	57.21	30.92	73.72		
	g	8.00	8.6	50	100	50	0.12	0.12	300	100	150	0.32	400	29.85	8.14	78.30		
	h	10.00	9.90	10	10	80	0.020	0.079	100	400	90	0.10	500	83.47	28.00	44.52		
	i	8.00	9.00	35	30	10	0	0.059	100	100	40	0.06	200	19.73	6.96	87.23		
	k	9.80	9.80	16	30	30	0.079	0.020	0	150	60	0.10	150	70.85	6.83	35.98		
Centroid of all points except b, which has the highest function value.																		
x_c		9.31	9.42	27.44	43.33	43.33	0.073	0.068	133.33	144.44	87	0.14	278	_	_	_	_	_
Reflexion of b through the centroid																		
$x_{r,1}$		9.97	9.64	21.17	30.00	50.00	0.089	0.063	100.00	91.67	80.00	0.15	191.67	64.58	4.50	39.92	_	_
Next		$f(i) < f(x_{r,1}) < f(b)$**: Replacement of b by** $x_{r,1}$																

Table 21
Vertices parameter values, function evaluations, and transformation calculations for Iteration 2 of the full scheme.

It.	Point	pH rougher [-]	pH cleaner [-]	Quebracho dosage (g/t)	Collector dosage rougher (g/t)	Collecor dosage cleaner (g/t)	Frother dosage rougher (mmol/L)	Frother dosage cleaner (mmol/L)	CS dosage rougher (g/t)	CS dosage cleaner (g/t)	Sum collector dosage (g/t)	Sum frother dosage (mmol/L)	Sum CS dosage (g/t)	Scheelite recovery (%)	Calcite recovery (%)	$Sch_{rec.Tails} + Cal_{rec.Conc}$ (%)	Mean (%)	Std (%)
2	a	9.80	8.80	16	30	30	0.079	0.020	0	0	60	0.10	0	84.36	25.84	41.48	59.72	20.15
	$x_{r,1}$	9.97	9.64	22	30	50.00	0.089	0.063	100	92	80	0.15	192	64.58	4.50	39.92		
	c	10.00	10.00	65	50	50	0.079	0.079	300	50	100	0.16	350	14.20	3.07	86.87		
	d	9.20	10.00	25	30	60	0.119	0.040	250	100	90	0.16	350	75.43	34.94	59.51		
	e	10.00	9.20	30	40	50	0.059	0.079	0	250	90	0.14	250	65.73	15.39	49.66		
	f	9.000	9.50	0	70	30	0.099	0.040	150	150	100	0.14	300	57.21	30.92	73.72		
	g	8.0	8.60	50	100	50	0.119	0.198	300	100	150	0.32	400	29.85	8.14	78.30		
	h	10.00	9.900	10	10	80	0.020	0.079	100	400	90	0.10	500	83.47	28.00	44.52		
	i	8.00	9.00	35	30	10	0.000	0.059	100	100	40	0.06	200	19.73	6.96	87.23		
	k	9.80	9.8	16	30	30	0.079	0.020	0	150	60	0.10	150	70.85	6.83	35.98		
Centroid of all points except i, which has the highest function value.																		
	x_c	9.53	9.49	25.91	43.33	47.78	0.083	0.069	133.33	143.52	91.11	0.15	276.85	_	_			
Reflexion of i through the centroid																		
	$x_{r,2}$	10	9.74	21.36	50.00	66.67	0.12	0.073	150.00	165.28	116.67	0.20	315.28	75.95	7.06	31.11		
Expansion from x_c through $x_{r,2}$																		
	$x_{e,1}$	10	9.86	19.09	53.33	76.11	0.14	0.075	158.33	176.16	129.44	0.22	334.49	68.18	8.34	40.14		
Next		$f(x_{e,1}) > f(x_{r,2})$**: Replacement of** i **by** $x_{r,2}$																

Table 22
Vertices parameter values and function evaluations for the simplex produced by iteration 2 of the full scheme.

It.	Point	pH rougher [-]	pH cleaner [-]	Quebracho dosage (g/t)	Collector dosage rougher (g/t)	Collecor dosage cleaner (g/t)	Frother dosage rougher (mmol/L)	Frother dosage cleaner (mmol/L)	CS dosage rougher (g/t)	CS dosage cleaner (g/t)	Sum collector dosage (g/t)	Sum frother dosage (mmol/L)	Sum CS dosage (g/t)	Scheelite recovery (%)	Calcite recovery (%)	$Sch_{rec.Tails} + Cal_{rec.Conc}$ (%)	Mean (%)	Std (%)
2	a	9.8	8.8	16	30	30	0.079	0.020	0	0	60	0.10	0	84.36	25.84	41.48	54.11	19.44
	$x_{r,1}$	9.97	9.64	21.17	30.00	50.00	0.089	0.063	100.00	91.67	80.00	0.15	191.67	64.58	4.50	39.92		
	c	10.0	10.0	65	50	50	0.079	0.079	300	50	100	0.16	350	14.20	3.07	86.87		
	d	9.2	10.0	25	30	60	0.12	0.040	250	100	90	0.16	350	75.43	34.94	59.51		
	e	10.0	9.2	30	40	50	0.059	0.079	0	250	90	0.14	250	65.73	15.39	49.66		
	f	9.0	9.5	0	70	30	0.099	0.040	150	150	100	0.14	300	57.21	30.92	73.72		
	g	8.0	8.6	50	100	50	0.12	0.20	300	100	150	0.32	400	29.85	8.14	78.30		
	h	10.0	9.9	10	10	80	0.020	0.079	100	400	90	0.10	500	83.47	28.00	44.52		
	$x_{r,2}$	10	9.74	21.36	50.00	66.67	0.12	0.073	150.00	165.28	116.67	0.20	315.28	75.95	7.06	31.11		
	k	9.8	9.8	16	30	30	0.079	0.020	0	150	60	0.10	150	70.85	6.83	35.98		
Mean of the parameter values		9.61	9.47	25.45	44.00	49.67	0.087	0.069	135.00	145.69	93.67	0.16	280.69					

Data availability

Data will be made available on request.

References

Ahn, H., Central Composite Design for the Experiments with Replicate Runs at Factorial and Axial Points, in Industrial Engineering, Management Science and Applications 20152015. p. 969-979.

Ann Bazar, J., Rahimi, M., Fathinia, S., Jafari, M., Chipakwe, V., Chehreh Chelgani, S., 2021. Talc Flotation—an Overview. Minerals. 11, 10.3390/min11070662.

Baudin, M., Nelder mead user's manual 2009.

Ben Said, B., L. Pereira, T. Saeed, D.H. Hoang, N. Kupka, R. Tolosana-Delgado, and M. Rudolph, Development of a user-friendly R Platform for Optimizing Mineral Processing, in International Mineral Processing Congress Asia-Pacific. 2022: Melbourne Australia.

Ben Said, B., L. Pereira, R. Tolosana-Delgado, and M. Rudolph, A user-friendly R Platform for Optimizing Mineral Processing (2022) Doi: 10.14278/rodare.1509.

Ben Said, B., Rudolph, M., Ebert, D., Goldmann, D., Pereira, L., 2024. Nanoparticle depressants in froth flotation – The effect of colloidal silica with different size and surface modifications on the selective separation of semi-soluble salt type minerals. Colloids Surf. A Physicochem. Eng. Asp. 690. https://doi.org/10.1016/j.colsurfa.2024.133697.

Deng, R., Huang, Y., Hu, Y., Ku, J., Zuo, W., Yin, W., 2018. Study of reverse flotation of calcite from scheelite in acidic media. Appl. Surf. Sci. 439, 139–147. https://doi.org/10.1016/j.apsusc.2017.12.231.

Dong, Z., Wang, R., Fan, M., Fu, X., 2017. Switching and optimizing control for coal flotation process based on a hybrid model. PLoS One 12, e0186553. https://doi.org/10.1371/journal.pone.0186553.

Drzymala, J., Luszczkiewicz, A., Foszcz, D., 2010. Application of Upgrading Curves for Evaluation of Past, Present, and Future Performance of a Separation Plant. Miner. Process. Extr. Metall. Rev. 31, 165–175. https://doi.org/10.1080/08905436.2010.482858.

Drzymala, J., Kowalczuk, P.B., Oteng-Peprah, M., Foszcz, D., Muszer, A., Henc, T., Luszczkiewicz, A., 2013. Application of the grade-recovery curve in the batch flotation of Polish copper ore. Miner. Eng. 49, 17–23. https://doi.org/10.1016/j.mineng.2013.04.024.

Durakovic, B., 2017. Design of experiments application, concepts, examples: State of the art. Periodicals Eng. Natural Sci. (PEN). 5. https://doi.org/10.21533/pen.v5i3.145.

Erkan, E., Ekmekçi, Z., Altun, E., 2022. Comparison Of flash flotation and gravity separation performance in a greenfield gold project. Physicochem. Probl. Miner. Process., 10.37190/ppmp/146979

Evans, C., Coulter, B., Wightman, E., Burrows, A., 2009. Improving Energy efficiency across mineral processing and smelting operations – a new approach. SDIMI Conf.

Fandrich, R., Gu, Y., Burrows, D., Moeller, K., 2007. Modern SEM-based mineral liberation analysis. Int. J. Miner. Process. 84, 310–320. https://doi.org/10.1016/j.minpro.2006.07.018.

Gao, Z., Zawala, J., Kowalczuk, P.B., 2020. Editorial: Surface Chemistry of Flotation. Front. Mater. 7. https://doi.org/10.3389/fmats.2020.595146.

Gaudin, A.M., 1939. Principles of Mineral Dressing, first ed. McGraw-Hill Book Company, inc., New York, London.
Jang, H., Topal, E., 2020. Transformation of the Australian mining industry and future prospects. Min. Technol. 129, 120–134. https://doi.org/10.1080/25726668.2020.1786298.
Kalyani, V.K., Pallavika, T. Gouri Charan, and S. Chaudhuri, Optimization of a Laboratory-Scale Froth Flotation Process Using Response Surface Methodology, Coal Preparation. 25 (2005) 141-153. 10.1080/07349340590962793.
Kupka, N., Babel, B., Rudolph, M., 2020. The potential role of colloidal silica as a depressant in Scheelite flotation. Minerals. 10, 144. https://doi.org/10.3390/min10020144.
Loveday, B.K., Brouckaert, C.J., 1995. An analysis of flotation circuit design principles. Chem. Eng. J. Biochem. Eng. J. 59, 15–21. https://doi.org/10.1016/0923-0467(95)03001-8.
Lu, F., Gui, W., Yang, C., Wang, X., 2022. Two-Step Optimal-Setting Control for Reagent Addition in Froth Flotation Based on Belief Rule Base. Processes. 10. https://doi.org/10.3390/pr10101933.
Lu, F., Liu, H., Lv, W., 2023. Prediction of Clean Coal Ash Content in Coal Flotation through a Convergent Model Unifying Deep Learning and Likelihood Function, Incorporating Froth Velocity and Reagent Dosage Parameters. Processes. 11. https://doi.org/10.3390/pr11123425.
Maldonado, M., Sbarbaro, D., Lizama, E., 2007. Optimal control of a rougher flotation process based on dynamic programming. Miner. Eng. 20, 221–232. https://doi.org/10.1016/j.mineng.2006.08.015.
Martínez-L, A., A. Uribe S, F.R. Carrillo P, J. Coreño A, and J.C. Ortiz, Study of celestite flotation efficiency using sodium dodecyl sulfonate collector: factorial experiment and statistical analysis of data, Int. J. Miner. Process. 70 (2003) 83-97. 10.1016/s0301-7516(02)00152-7.
Nagaraj, D.R., 2005. Reagent selection and optimization—the case for a holistic approach. Miner. Eng. 18, 151–158. https://doi.org/10.1016/j.mineng.2004.10.017.
Napier-Munn, T.J., 1998. Analysing plant trials by comparing recovery-grade regression lines. Miner. Eng. 11, 949–958. https://doi.org/10.1016/S0892-6875(98)00082-X.
Napier-Munn, T.J., 2012. Statistical methods to compare batch flotation grade-recovery curves and rate constants. Miner. Eng. 34, 70–77. https://doi.org/10.1016/j.mineng.2012.03.036.
Neethling, S.J., Cilliers, J.J., 2012. Grade-recovery curves: A new approach for analysis of and predicting from plant data. Miner. Eng. 36–38, 105–110. https://doi.org/10.1016/j.mineng.2012.02.018.
Nelder, J.A., Mead, R., 1965. A simplex method for function minimization. Comput. J. 7, 308–313. https://doi.org/10.1093/comjnl/7.4.308.
Nuorivaara, T., Bjorkqvist, A., Bacher, J., Serna-Guerrero, R., 2019. Environmental remediation of sulfidic tailings with froth flotation: Reducing the consumption of additional resources by optimization of conditioning parameters and water recycling. J. Environ. Manage. 236, 125–133. https://doi.org/10.1016/j.jenvman.2019.01.107.
Sajjad, M., Otsuki, A., 2022. Correlation between Flotation and Rheology of Fine Particle Suspensions. Metals. 12. https://doi.org/10.3390/met12020270.
Sheridan, M.S., Nagaraj, D.R., Fornasiero, D., Ralston, J., 2002. The use of a factorial experimental design to study collector properties of N-allyl-O-alkyl thionocarbamate collector in the flotation of a copper ore. Miner. Eng. 15, 333–340. https://doi.org/10.1016/S0892-6875(02)00037-7.
Stanujkić, D., Milanović, D., Magdalinović, S., Jovanović, I., 2017. An approach to the evaluation of froth flotation reagents based on the use of the SWARA and WS-PLP methods. Mining Metall. Eng. Bor. 103–110. https://doi.org/10.5937/mmeb1704103S.
Szmigiel, A., Apel, D.B., Skrzypkowski, K., Wojtecki, L., Pu, Y., 2024. Advancements in Machine Learning for Optimal Performance in Flotation Processes: A Review. Minerals. 14. https://doi.org/10.3390/min14040331.
Tijsseling, L.T., Dehaine, Q., Rollinson, G.K., Glass, H.J., 2020. Mineralogical Prediction of Flotation Performance for a Sediment-Hosted Copper–Cobalt Sulphide Ore. Minerals. 10. https://doi.org/10.3390/min10050474.
Wan, K., Xu, D., Cai, Y., 2021. Data-driven-based model predictive control of reagents addition for tungsten flotation process. In: In 2021 China Automation Congress (CAC), pp. 1629–1634.
Xie, Y., Cao, B., He, Y., Yang, C., Gui, W., 2016. Reagent dosages control based on bubble size characteristics for flotation process. IET Control Theory Appl. 10, 1404–1411. https://doi.org/10.1049/iet-cta.2015.0839.
Yan, S., Zhang, J.Q., Diao, W.Z., 2013. Flotation Reagent Progress and Application Overview. Appl. Mech. Mater. 441, 76–79. https://doi.org/10.4028/www.scientific.net/AMM.441.76.